

595034
P. 66

The Propulsive Small Expendable Deployer System (ProSEDS)

NASA Grant NAG8-1605

Annual Report #3

For the period 1 August 2001 through 31 July 2002

Principal Investigator

Enrico C. Lorenzini

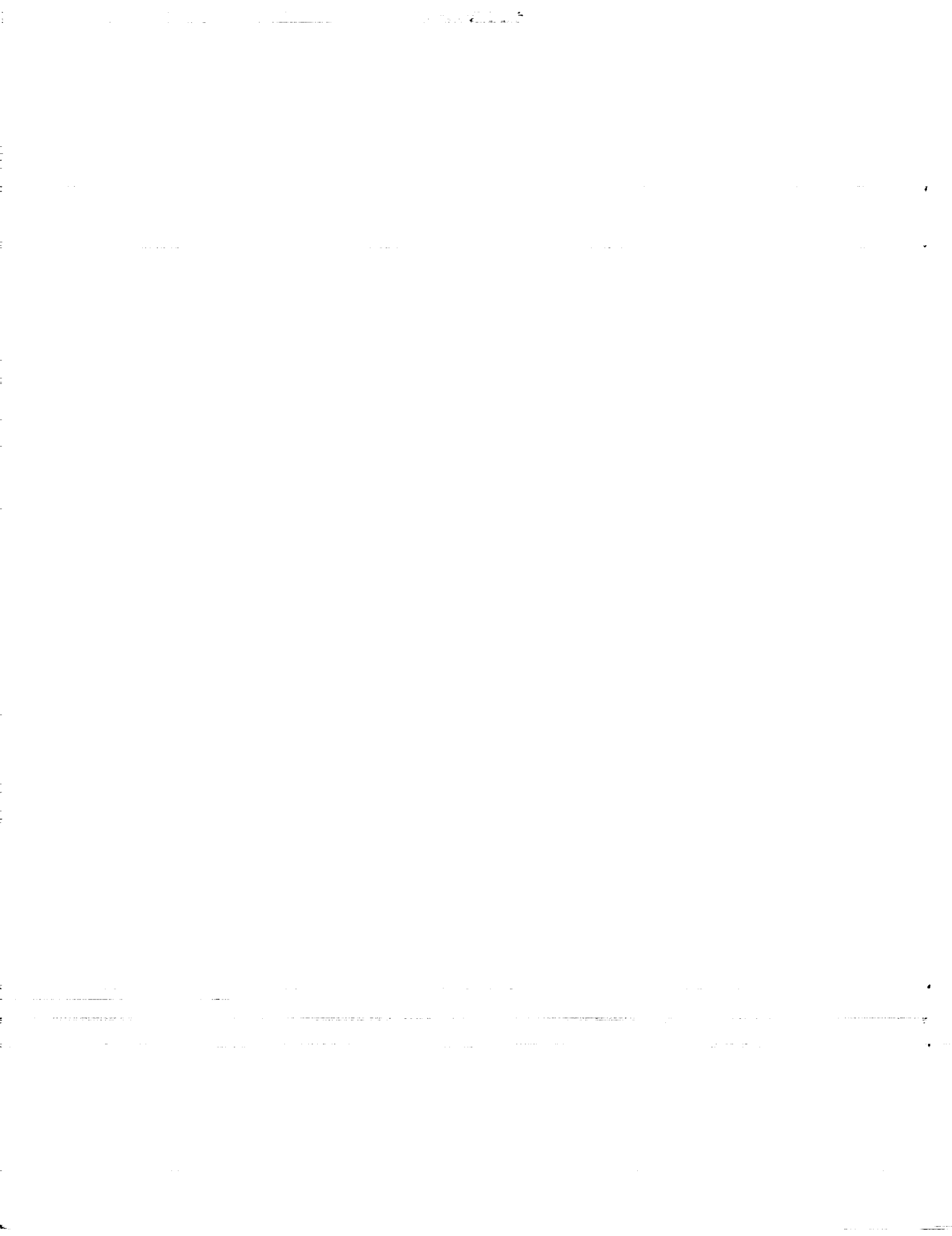
July 2002

Prepared for

National Aeronautics and Space Administration
Marshall Space Flight Center, Alabama 35812

Smithsonian Institution
Astrophysical Observatory
Cambridge, Massachusetts 02138

The Smithsonian Astrophysical Observatory
is a member of the
Harvard-Smithsonian Center for Astrophysics



The Propulsive Small Expendable Deployer System (ProSEDS)

NASA Grant NAG8-1605

Annual Report #3

For the period 1 August 2001 through 31 July 2002

Principal Investigator

Enrico C. Lorenzini

Co-Investigators

Mario L. Cosmo

Collaborators

Juan Sanmartin

Jesus Peláez

July 2002

Prepared for

National Aeronautics and Space Administration

Marshall Space Flight Center, Alabama 35812

Smithsonian Institution

Astrophysical Observatory

Cambridge, Massachusetts 02138

The Smithsonian Astrophysical Observatory

is a member of the

Harvard-Smithsonian Center for Astrophysics

TABLE OF CONTENTS

LIST OF FIGURES.....	2
LIST OF TABLES	3
SCOPE.....	4
SUMMARY	5
1. UPDATED REFERENCE MISSION.....	6
1.1 INTRODUCTION.....	6
1.2 NEW MISSION PARAMETERS AND CURRENT OPERATING CYCLES.....	7
1.3 APPLICABILITY OF RESULTS TO LATER LAUNCH DATES.....	15
1.4 EXTREME ELECTRODYNAMIC FORCING	17
1.5 CONCLUDING REMARKS.....	23
2.0 EVALUATION OF POWER DELIVERED BY THE TETHER.....	24
2.1 INTRODUCTION.....	24
2.2 NUMERICAL RESULTS	24
2.3 CONCLUDING REMARKS.....	25
3.0 UPDATED DEPLOYMENT CONTROL PROFILES AND SIMULATIONS.....	26
3.1 INTRODUCTION.....	26
3.2 FRICTION MODEL.....	27
3.3 FLIGHT REFERENCE TABLE.....	29
3.4 FLIGHT CONTROL LAW PARAMETERS.....	34
3.5 SENSITIVITY OF CONTROL LAW TO FRICTION PARAMETERS	37
3.6 CONCLUDING REMARKS	44
4.0 ANALYSIS/ESTIMATION OF DEPLOYMENT FLIGHT DATA	45
4.1 INTRODUCTION.....	45
4.2 NUMERICAL RESULTS.....	46
4.3 CONCLUDING REMARKS	47
APPENDIX A.....	48
REFERENCES.....	64

LIST OF FIGURES

Figure 1 Schematic of ProSEDS on Delta 2 nd stage	6
Figure 2 Operating cycle #1 (60-sec cycle) - Operation on Primary Battery.....	8
Figure 3 New operating cycle #2 (80-sec cycle) - Operation on Secondary Battery	8
Figure 4 Simulation results for Summer 2002 launch; nominal solar condition.....	10
Figure 5 Simulation results for Summer 2002 launch; nominal solar condition.....	11
Figure 6 Simulation results for Summer 2002 launch; nominal solar condition.....	12
Figure 7 Simulation results for Summer 2002 launch; nominal solar condition.....	13
Figure 8 Simulation results for Summer 2002 launch; nominal solar condition.....	14
Figure 9 Sunspot number predictions [NASA MSFC].....	16
Figure 10 Ionospheric Global Index (IG) prediction [Rutherford Appleton laboratory].....	16
Figure 11 Results for Summer 2002 launch, plasma density twice nominal.....	18
Figure 12 Results for Summer 2002 launch, plasma density twice nominal.....	19
Figure 13 Results for Summer 2002 launch, plasma density twice nominal.....	20
Figure 14 Results for Summer 2002 launch, plasma density twice nominal.....	21
Figure 15 Results for Summer 2002 launch, plasma density twice nominal.....	22
Fig. 16 Tether current during battery charging mode: instant value and 12-hour average...	24
Figure 17 Control law Reference Profile #78.....	34
Figure 18 Deployment dynamics for Ref#78 and $T_0 = 5$ mN.....	39
Figure 19 Deployment dynamics for Ref#78 and $T_0 = 10$ mN.....	40
Figure 20 Deployment dynamics for Ref#78 and $T_0 = 20$ mN (reference).....	41
Figure 21 Deployment dynamics for $T_0 = 20$ mN with $\pm 50\%$ <i>tension white noise</i>	42
Figure 22 Deployment trajectory of the endmass with respect to the Delta stage.....	43
Figure 23 Final libration amplitude vs. T_0 with control (Ref. #78) and without control.....	44
Figure 24 Deployment trajectory of endmass: estimated from noisy turn counter data (solid line); and original data (dotted line).....	46

LIST OF TABLES

Table 1 Updated control parameters for Reference Profile #78.....36

SCOPE

This is the Annual Report #3 for Grant NAG8-1605 entitled “The Propulsive Small Expendable Deployer System (ProSEDS)” prepared by the Smithsonian Astrophysical Observatory for NASA Marshall Space Flight Center. This report covers the period of activity from 1 August 2001 through 30 July 2002. The technical officer for this grant is Leslie Curtis at NASA MSFC.

SUMMARY

This Annual Report covers the following main topics:

1. Updated Reference Mission

The reference ProSEDS mission is evaluated for an updated launch date in the Summer of 2002 and for the new 80-s current operating cycle. Simulations are run for nominal solar activity condition at the time of launch and for extreme conditions of dynamic forcing. Simulations include the dynamics of the system, the electrodynamics of the bare tether, the neutral atmosphere and the thermal response of the tether.

2. Evaluation of power delivered by the tether system

The power delivered by the tethered system during the battery charging mode is computed under the assumption of minimum solar activity for the new launch date.

3. Updated Deployment Control Profiles and Simulations

A number of new deployment profiles were derived based on the latest results of the deployment ground tests. The flight profile is then derived based on the friction characteristics obtained from the deployment tests of the F-1 tether.

4. Analysis/estimation of deployment flight data

A process was developed to estimate the deployment trajectory of the endmass with respect to the Delta and the final libration amplitude from the data of the deployer turn counters. This software was tested successfully during the ProSEDS mission simulation at MSFC EDAC.

1. UPDATED REFERENCE MISSION

1.1 Introduction

We recall in this brief introduction a few general information about the Propulsive Small Expendable Deployment System (ProSEDS) in order to spare the reader from looking up this basic information in other documents. ProSEDS will carry out a demonstration of a bare electrodynamic tether for propulsion. The system will fly as a secondary payload on a Delta II and it will be deployed from the 2nd stage (see Fig. 1). The electrodynamic forces generated by the current flowing in the conductive tether are expected to strongly increase the decay rate of the Delta stage. The reader should consult references^{1 2 3 4 5} for a more detailed description of ProSEDS and the principles of operation of bare-tether anodes.

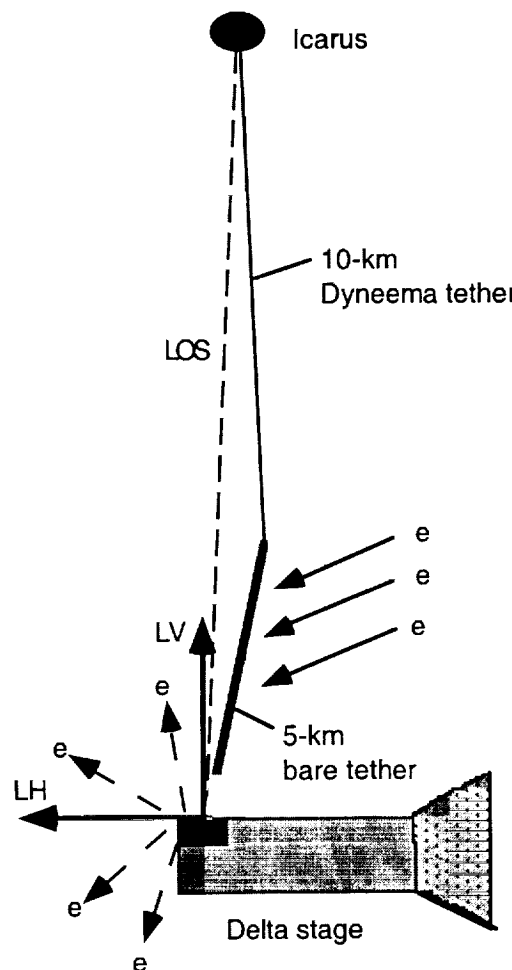


Figure 1 Schematic of ProSEDS on Delta 2nd stage

Electrons are collected along the upper portion of the bare tether which is positively biased with respect to the surrounding plasma. They are then reemitted into the ionosphere at the Delta stage by an active hollow cathode device. The (electronic) current flowing along the tether from its top to the bottom interacts with the Earth's magnetic field to produce an electrodynamic drag force which decreases the orbit of the Delta stage.

The performance of ProSEDS will be assessed on the basis of the decay rate of the Delta stage which is affected (for a given tether design) by the plasma conditions at mission time. The launch date of ProSEDS has changed throughout its development with the latest launch date being in the Summer of 2002. Moreover, the modes of operation of the tether current (i.e., the operating cycle) have also changed, as explained later on, resulting in a strongly increased decay rate.

1.2 New Mission Parameters and Current Operating Cycles

The ProSEDS mission had some notable changes in terms of launch date, starting altitude and current operating cycle. The launch date was moved to the Summer of 2002, the starting altitude was decreased from 400 km to roughly 360 km and the secondary operating cycle (with 80-s period) now consists of 50-s battery charging and 30-s shunt mode (see Fig. 3). The original primary cycle (with 60-s period as shown in Fig. 2) is utilized during the first 5 orbits while the secondary cycle is utilized thereafter.

The reference mission for the scheduled launch date of July 25th, 2002 is analyzed in the following. The new launch date impacts the system performance because the current in the tether is a function of the plasma density which, in turn, is a function of the solar activity. Consequently, the electrodynamic drag force and the reentry time change because of the changed plasma conditions. We are presently in solar cycle 23 with the solar activity going down towards a minimum of activity currently estimated to happen around the years 2007-2008. More importantly the ProSEDS tether current operating cycle has been changed. The older cycle consisted of 7 orbits of primary operating cycle followed by a secondary cycle. The old secondary cycle consisted of 35-s open circuit mode, 5-s resistor mode, 5-s shunt mode and 35-s battery charging mode. The new secondary operating cycle consists of 30-s shunt mode and 50-s battery charging mode. The change has a positive effect (as shown later on) on the decay rate of the orbit because there are no periods in the secondary operating cycle in which the tether current is off (open circuit mode) or severely limited (high resistor mode).

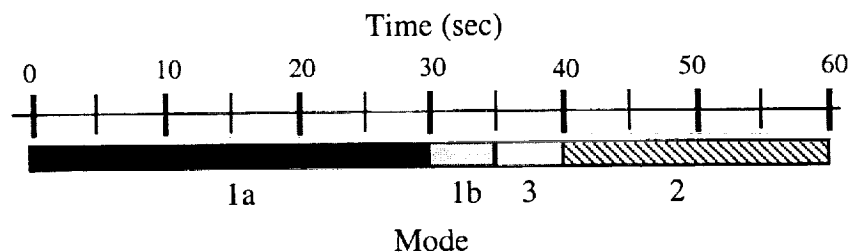


Figure 2 Operating cycle #1 (60-sec cycle) - Operation on Primary Battery

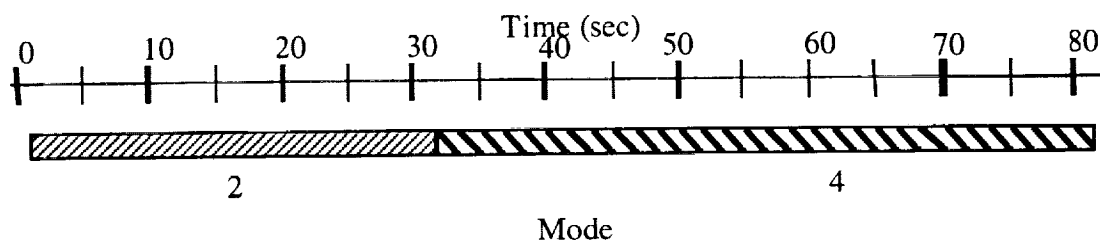


Figure 3 New operating cycle #2 (80-sec cycle) - Operation on Secondary Battery

Mode 1a is open circuit, plasma contactor OFF

Mode 1b is open circuit, plasma contactor ON

Mode 2 is SHUNT mode

Mode 3 is RESISTOR mode

Mode 4 is BATTERY CHARGE mode

Operating cycle #1 is on primary battery (first 5 orbits)

New operating cycle #2 is on secondary battery (after the first 5 orbits)

In the following, we show the results of the new reference mission simulation. The initial conditions and orbital parameters assumed for the reference simulation are as follows:

Launch date and time:

25 July 2002; UTC = 00:15:00 hr:min:s (at first perigee pass)

Orbital elements (from Boeing):

Semimajor axis = 6736.556794 km

Eccentricity = 0.001305

(Initial orbit approx: 350 km x 367 km, with respect to a spherical Earth)

Inclination = 35.363 deg

Right Ascension (RAAN) = 60.296 deg

Argument of perigee = 289.996 deg

Simulation started at first perigee pass, i.e., true anomaly = 0

Environmental conditions:

Nominal solar activity (50% percentile): $R_z = 94$ (SunSpot Number); $IG = 132$ (Ionospheric Global Index); $F_{10.7} = 141$ (radio flux), $A_p = 15$ (geomagnetic index).

System parameters:

Satellite mass = 21.4 kg;

Delta mass = 994 kg

Tether mass = 10-kg wire and 1.5-kg Dyneema

Wire external diameter = 1.2 mm

Dyneema average cross section: $\sim 1.2\text{mm} \times 0.2\text{mm}$

Tether optical properties:

Dyneema: $\alpha_s = 0.1$, $\epsilon_{IR} = 0.5$;

C-COR coated wire: $\alpha_s = 0.9$, $\epsilon_{IR} = 0.8$.

Tether mechanical properties: $EA = 15,000 \text{ N}$; $E'A \approx 2000 \text{ Ns}$.

Wire ohmic resistance = 250 ohm at 20 °C

Electrical operating cycle:

The primary cycle is activated at Delta Time = 12,666 s which corresponds to 4700 s after simulation start (when ProSEDS is off the coast of Brazil). The secondary cycle is activated after 5 orbits, i.e., at about 32,200 s after simulation start.

Results of the new reference mission simulation are shown in the following figures. Although these results have been computed for July 25, 2002, they are also valid throughout the Summer of 2002 because the ionospheric indexes change only a little over those months as explained in the next subsection.

ProSEDS 250 ohm@20 C, 350x367km, nom. solar, UTC 00:15:00, 25 July 2002

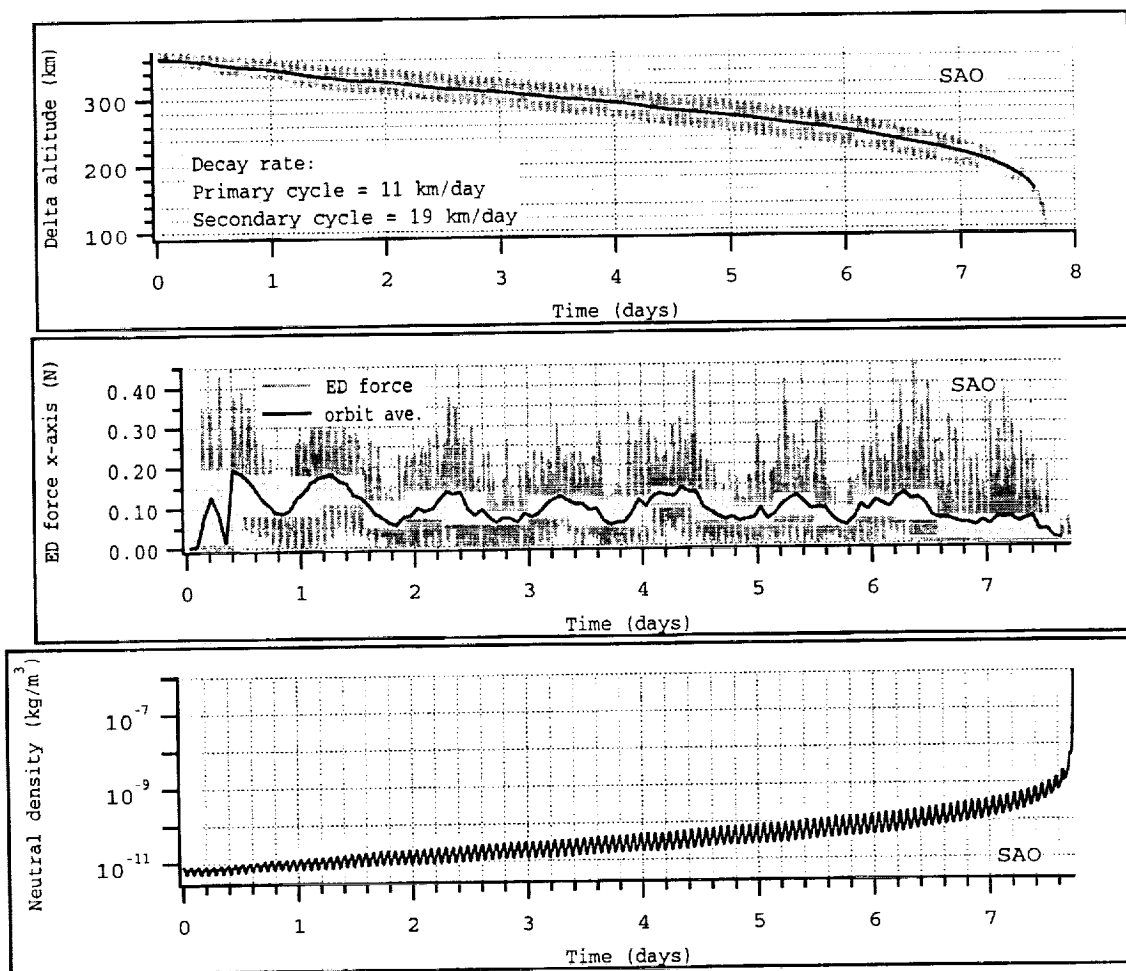


Figure 4 Simulation results for Summer 2002 launch; nominal solar condition

ProSEDS 250 ohm@20 C, 350x367km, nom. solar, UTC = 00:15:00, 25 July 2002

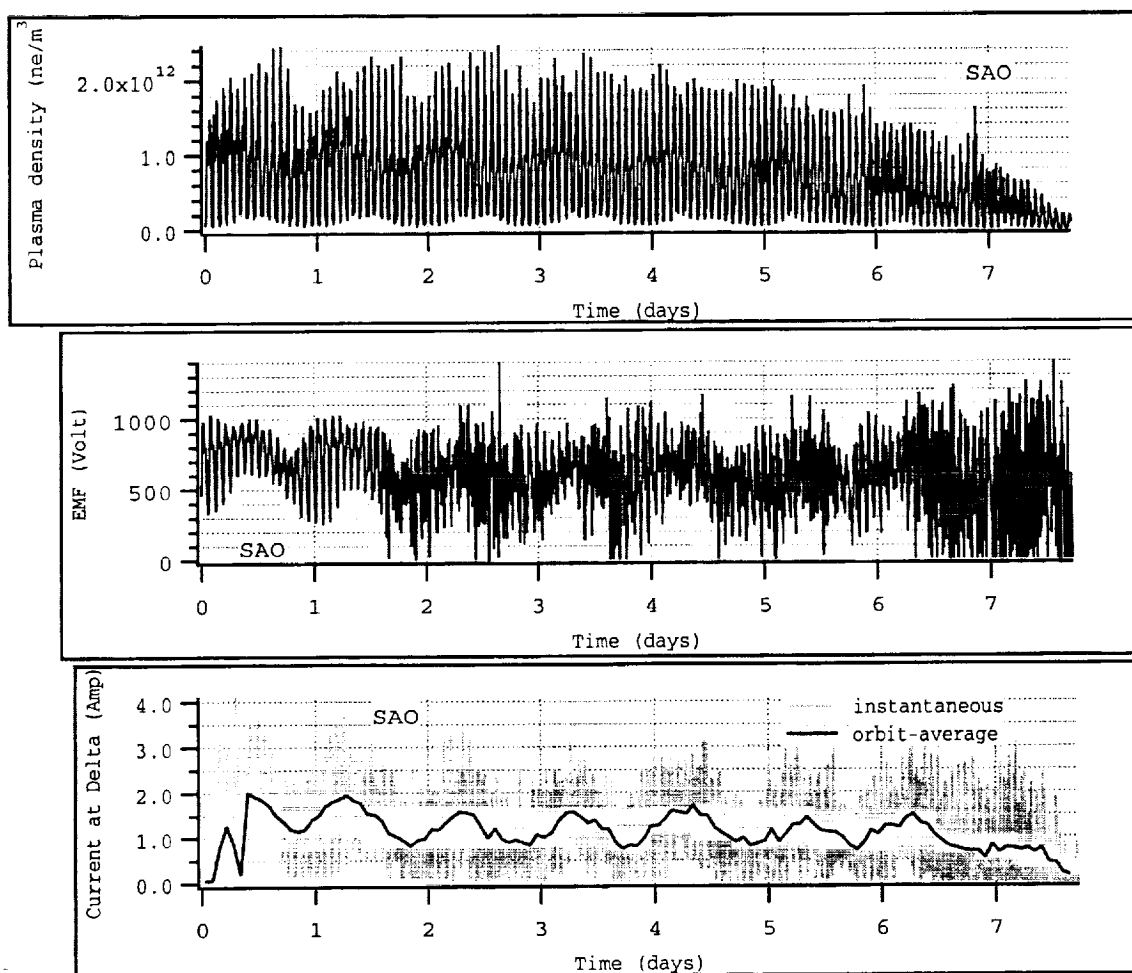


Figure 5 Simulation results for Summer 2002 launch; nominal solar condition

ProSEDS 250 ohm@20 C, 350x367km, nom. solar, UTC = 00:15:00, 7/25/2002

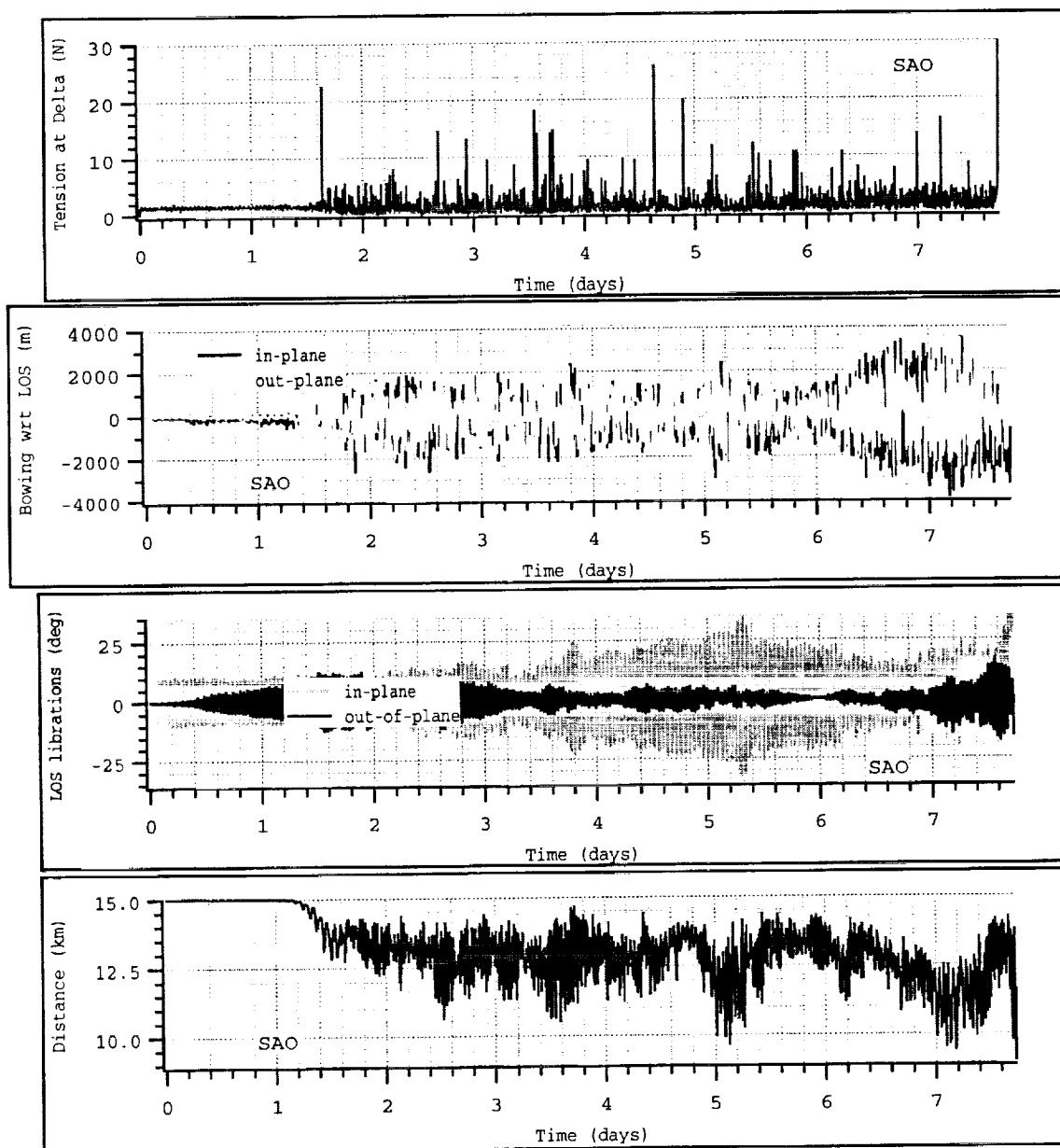


Figure 6 Simulation results for Summer 2002 launch; nominal solar condition

ProSEDS 250 ohm@20 C, 350x367km, nom. solar, UTC 00:15:00, 25 July 2002

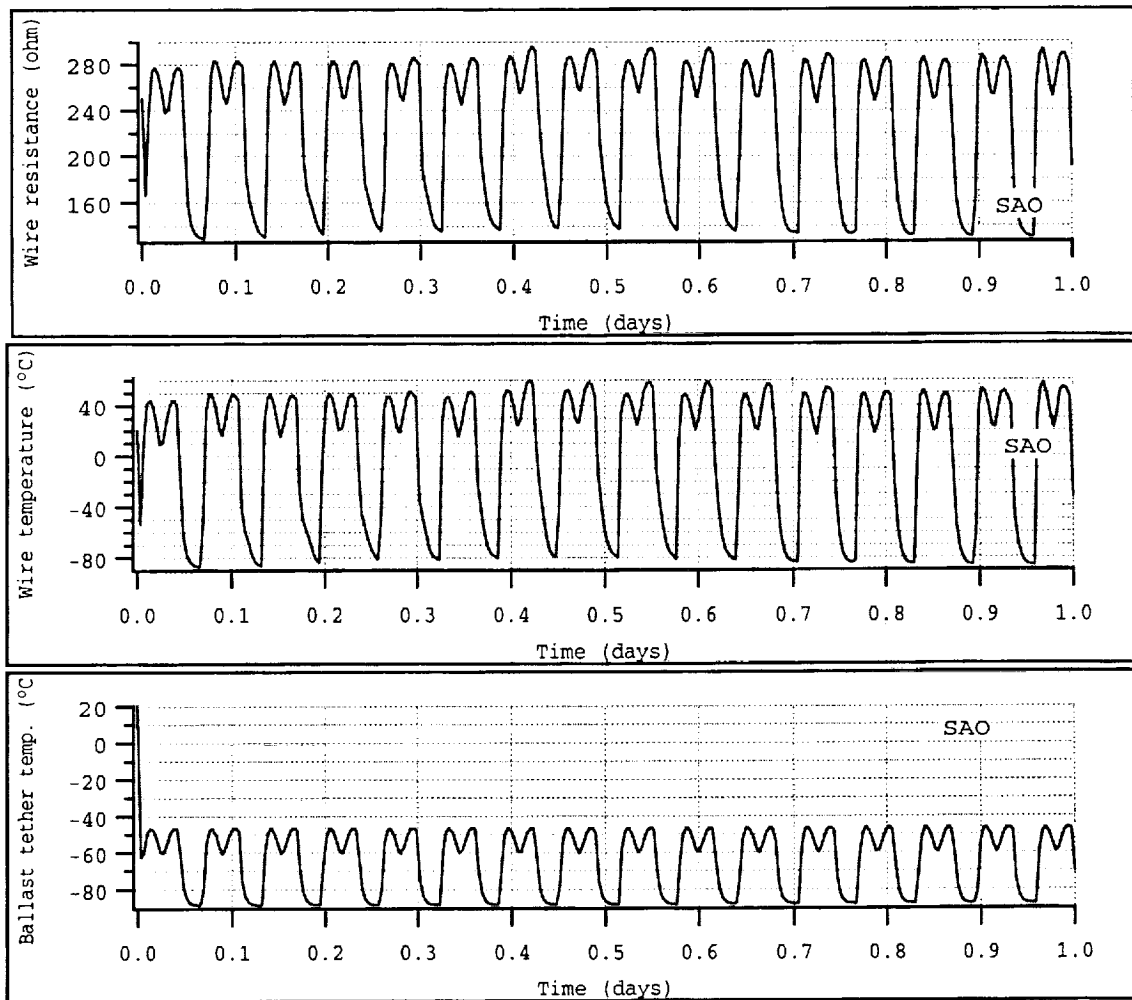


Figure 7 Simulation results for Summer 2002 launch; nominal solar condition

ProSEDS 250 ohm@20 C, 350x367km, nom. solar, UTC 00:15:00, 25 July 2002

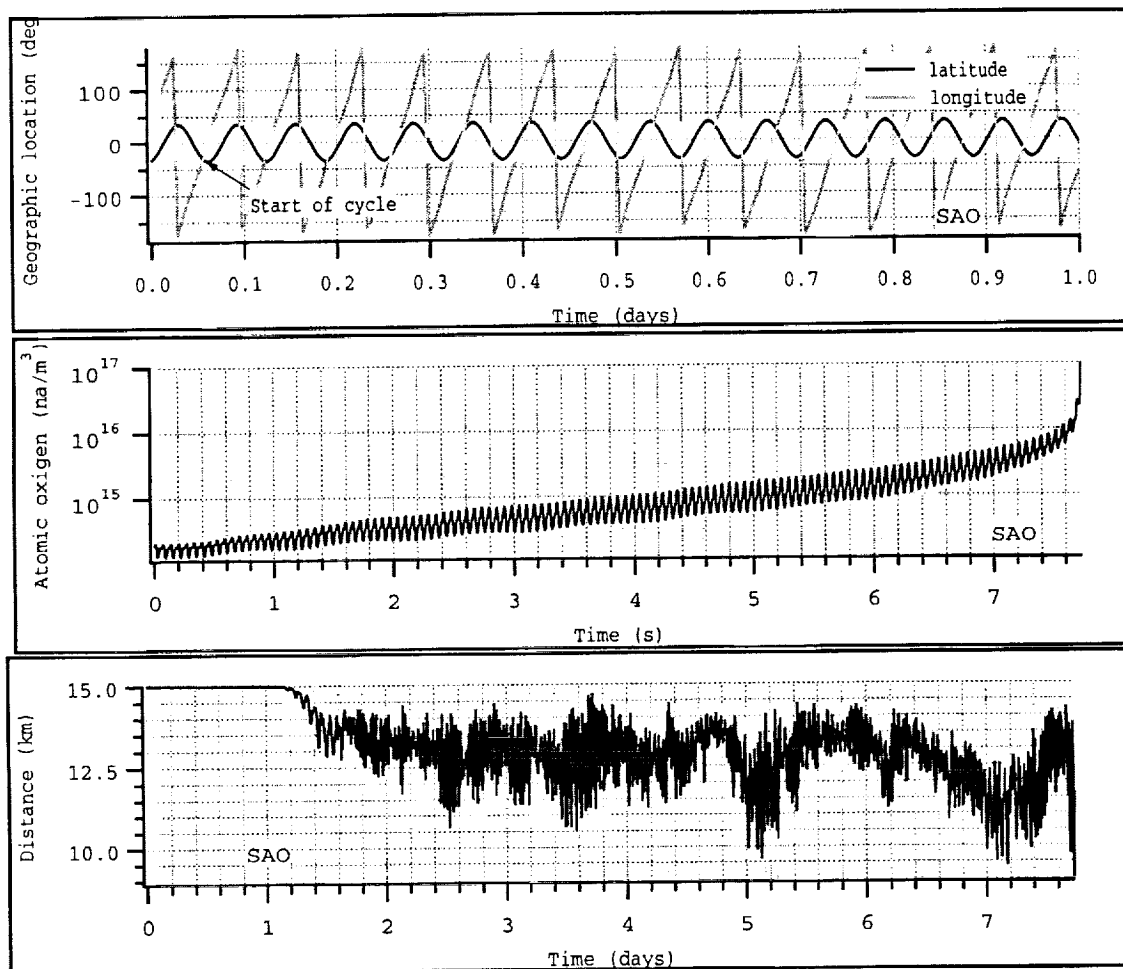


Figure 8 Simulation results for Summer 2002 launch; nominal solar condition

The results show that the new secondary operating cycle almost doubles the decay rate of ProSEDS with respect to previous scenarios. The system dynamics is also more strongly excited with the excitation increasing steeply after one day in orbit. The excitation is the result of a complex skip-rope motion in which the in-plane and out-of-plane motion are coupled as was studied in Refs. ⁶. The most noticeable indicator of this motion is the distance from the Delta to the end mass which is plotted in Figure 6. The fact that this distance does not go to zero suggests that the motion is not a planar motion but rather a coning motion resulting from a coupling between the in-plane and out-of plane degrees of freedom. The system dynamics is quite strong as it can be seen from Figure 6. The tension spikes in the tension plot result from recoiling after the tether has lost tension while there was a substantial shortening of the distance between the end mass and the Delta. The system, however, remains stable and it never topples over. The out-of-plane libration amplitude builds up to somewhat less than 30° at around 5.5 days and then decreases again; most likely because of an energy transfer between degrees of freedom.

If the tether were to remain intact (neglecting the effect of atomic oxygen and possibly a fatal micrometeoroid impact) the Delta stage would reenter the atmosphere before 8 days. However, this situation is only theoretical because the atomic oxygen will chew the Dyneema tether before the system encounters the dense atmosphere. The area below 250 km is where the Dyneema degradation due to atomic oxygen will become strong. The Dyneema tether will likely fail below that altitude, leaving the electrodynamic system in an uncertain state of functionality. Consequently, the rate of decay will slow down significantly after the tether severance with respect to the simulated decay rate that does not take a possible tether cut into account.

1.3 Applicability of results to later launch dates

We are presently in the solar cycle 23 during which the solar activity peaked in April-June 2000. Consequently, the solar activity and the plasma density (that is a function of the solar activity) will decrease over the next few years. The plasma density in the International Reference Ionosphere (IRI95) model is a function of two solar indexes (other than the point location): the Sun spot number (Rz) and the Ionospheric global index (IG). Figure 9 shows the prediction of the Sun spot number for this solar cycle and the next inclusive of high (95% percentile) and low (5% percentile) predicted values. Figure 10 shows the only available prediction of the Ionospheric global index (IG).

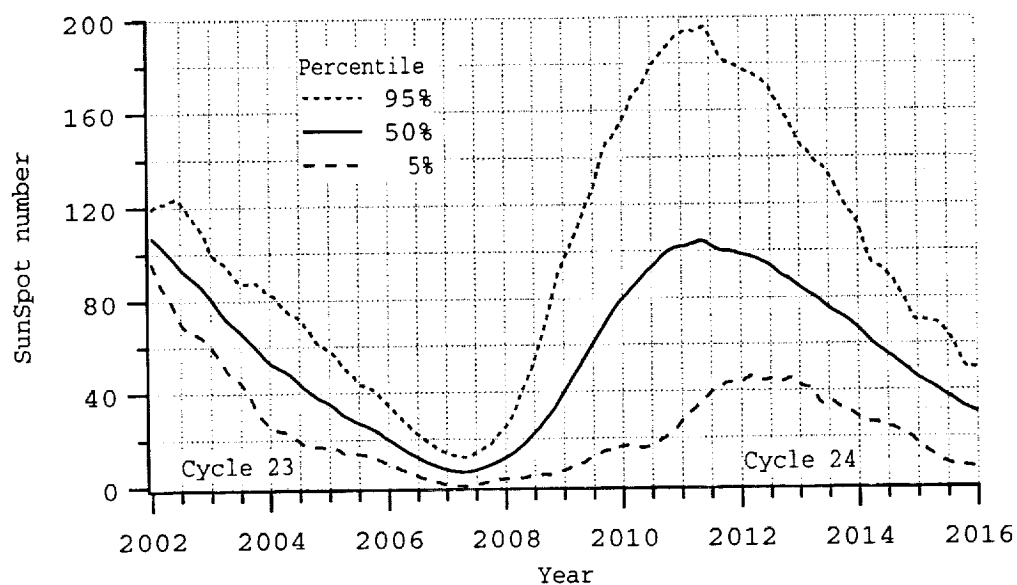


Figure 9 Sunspot number predictions [NASA MSFC]

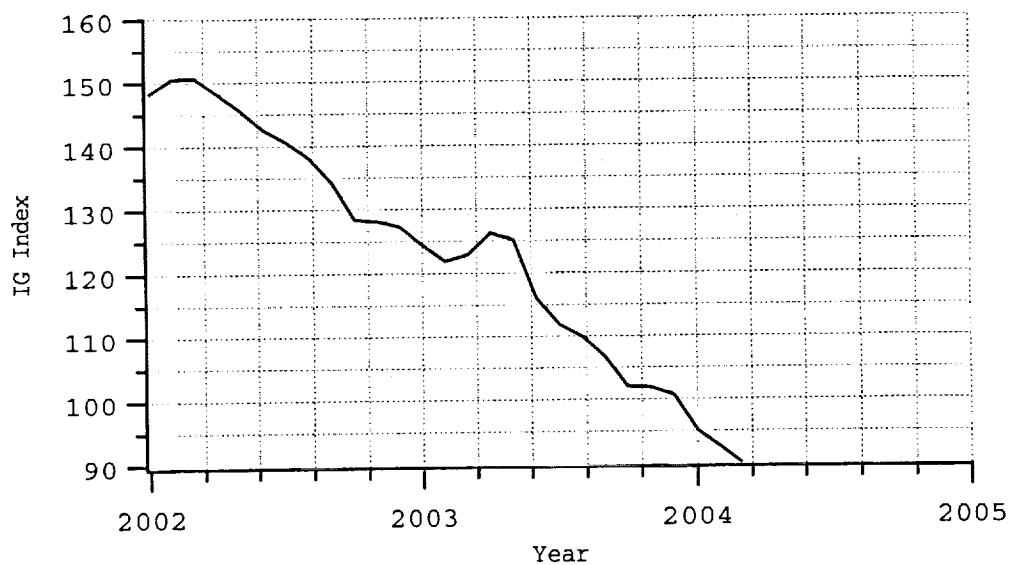


Figure 10 Ionospheric Global Index (IG) prediction [Rutherford Appleton laboratory]

The change of these two indexes over the 3 months of the Summer 2002 is fairly moderate and consequently the result of the July 25th simulation are valid in good approximation throughout the Summer of 2002.

1.4 Extreme electrodynamic forcing

For the purpose of evaluating the system behavior and stability under maximum forcing of the electrodynamic drag a case was run for a plasma density that is (artificially) twice the plasma density under nominal conditions.

The double plasma density increases the decay rate to 23 km/day averaged over six days of secondary cycle operation. Figures 11-15 show the response of the system under these extreme conditions of plasma density. It is notable that the decay rate does not double with respect to the baseline case thanks to the ability of the bare tether to adjust in part to changing plasma conditions.

The dynamic response of the system is stable. The growth of the in-plane libration is actually less than for nominal solar conditions. The higher growth of the in-plane libration in the nominal case was likely due to a transfer of energy from the out-of-plane to the in-plane degrees of freedom as it can be inferred from Figure 6. This points again to the strongly non-linear characteristics of this system dynamics. The loss of tether tension most likely plays a key role by changing the phase relationship among degrees of freedom and forcing terms after the tether rebound and consequently transferring energy from some oscillations to others in a fairly random fashion.

The conclusion is that the overall system stability is not impaired by a doubling of the plasma density.

ProSEDS 250 ohm@20 C, 360km, double plasma, 00:15:00UT 25, July 2002

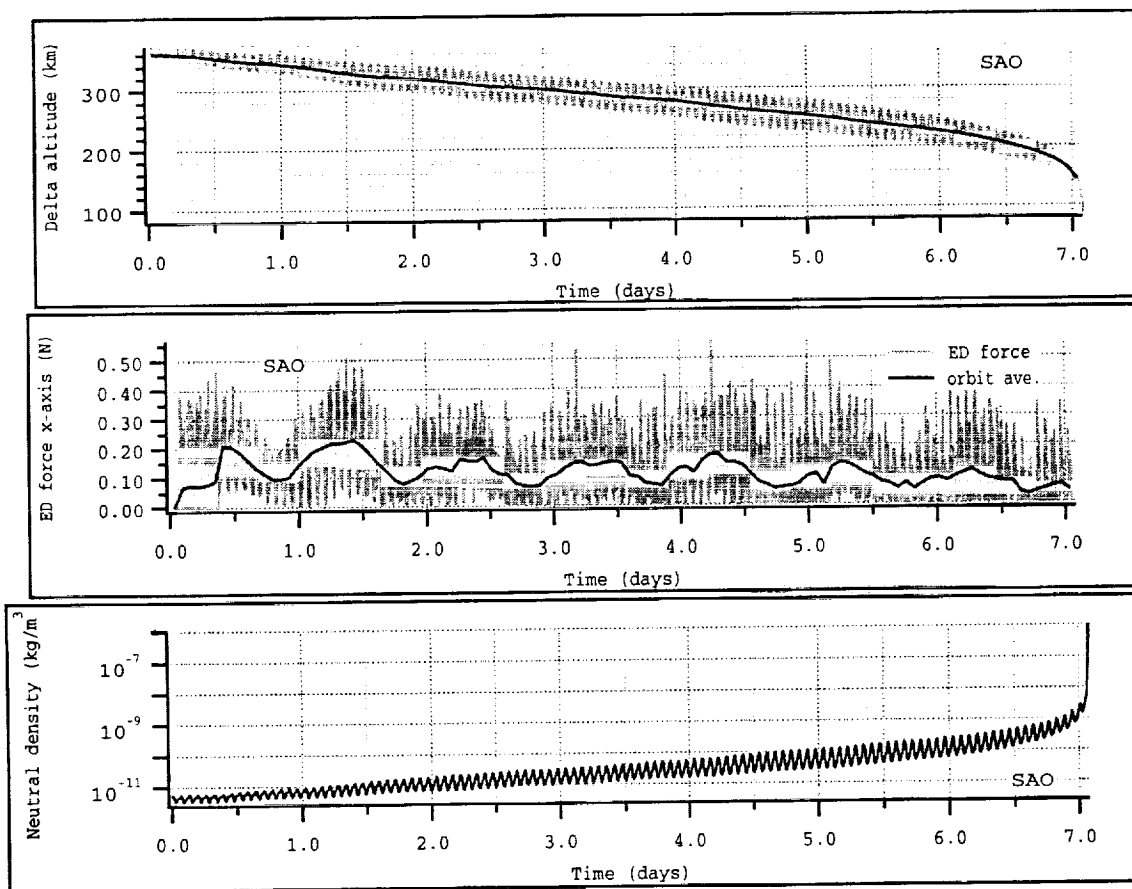


Figure 11 Results for Summer 2002 launch, plasma density twice nominal

ProSEDS 250 ohm@20 C, 360km, double plasma, 00:15:00UT, 25 July 2002

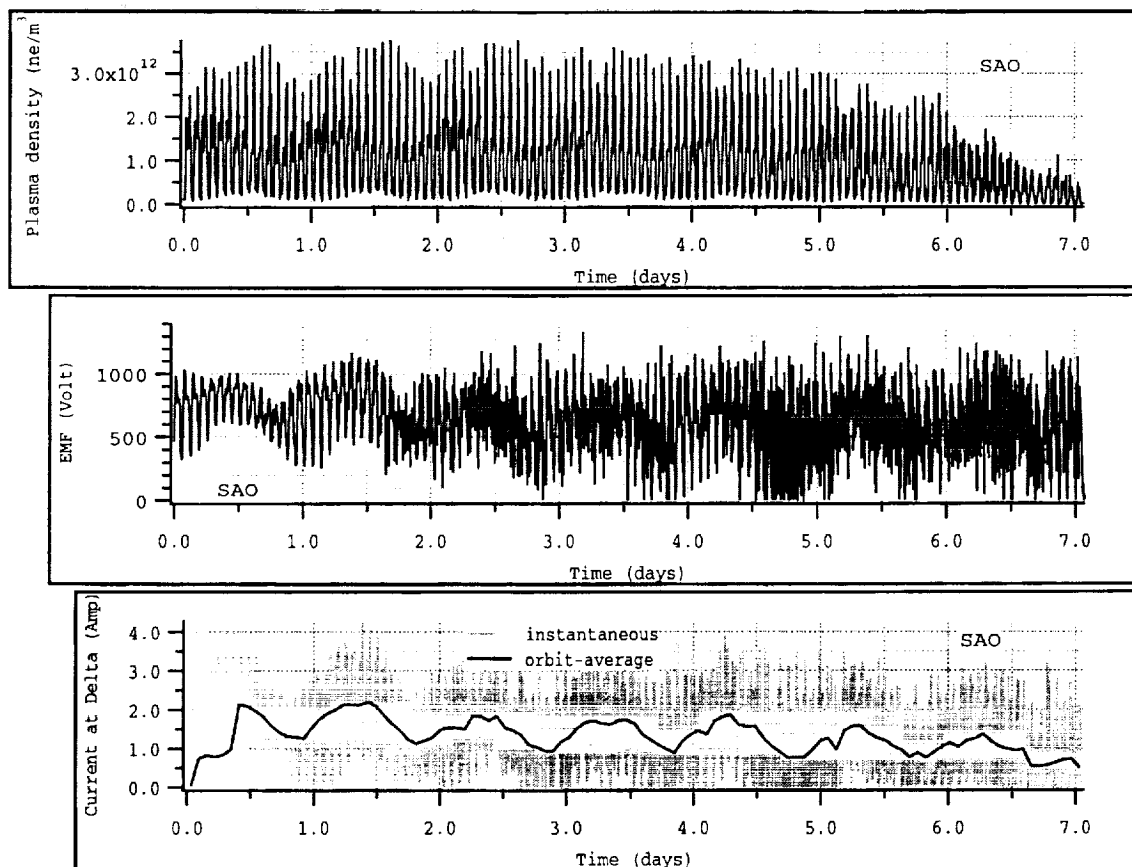


Figure 12 Results for Summer 2002 launch, plasma density twice nominal

ProSEDS 250 ohm@20 C, 360km, double plasma, 00:15:00UT, 25 July 2002

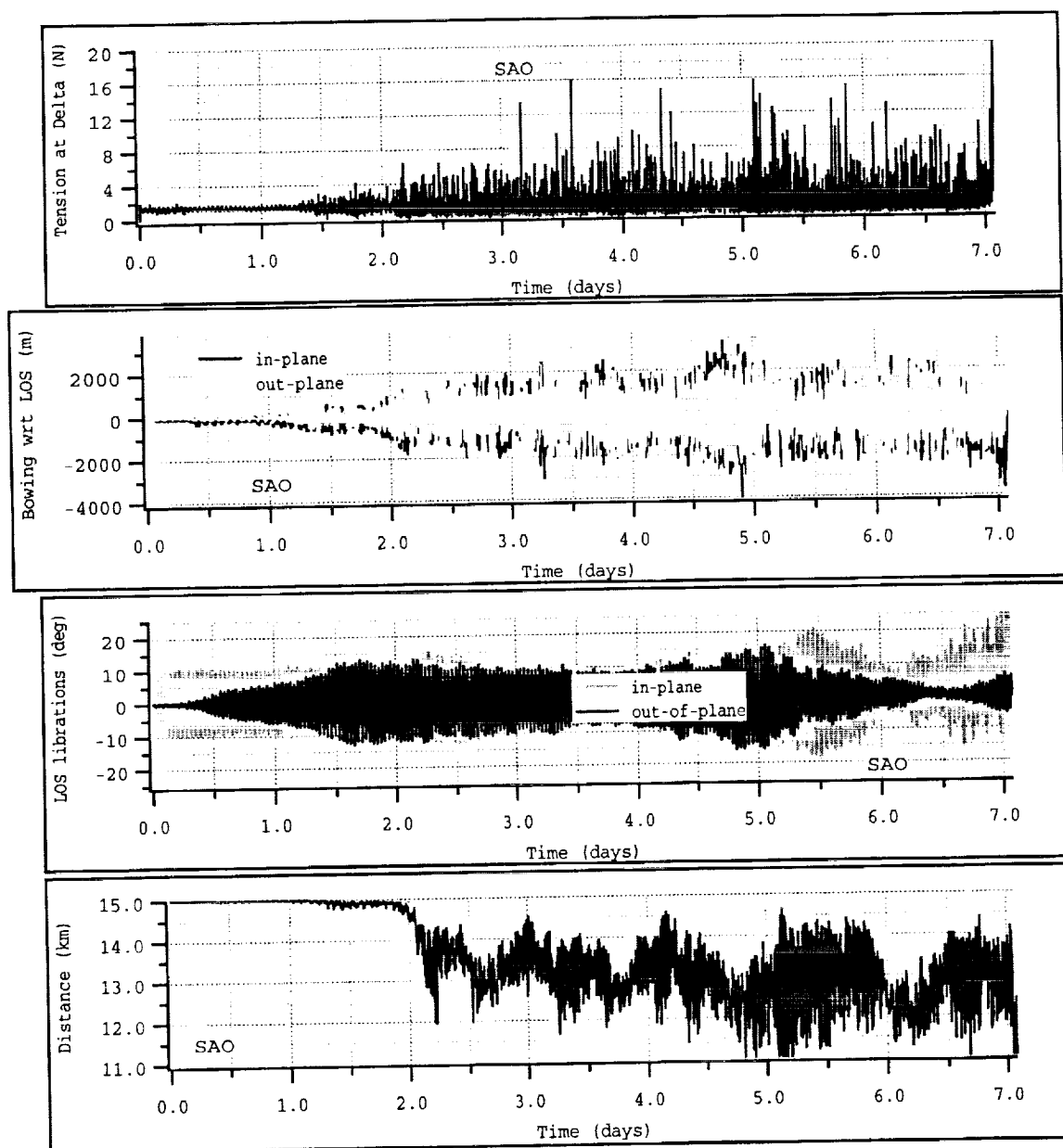


Figure 13 Results for Summer 2002 launch, plasma density twice nominal

ProSEDS 250 ohm@20 C, 360km, double plasma, 00:015:00T, 25 July 2002

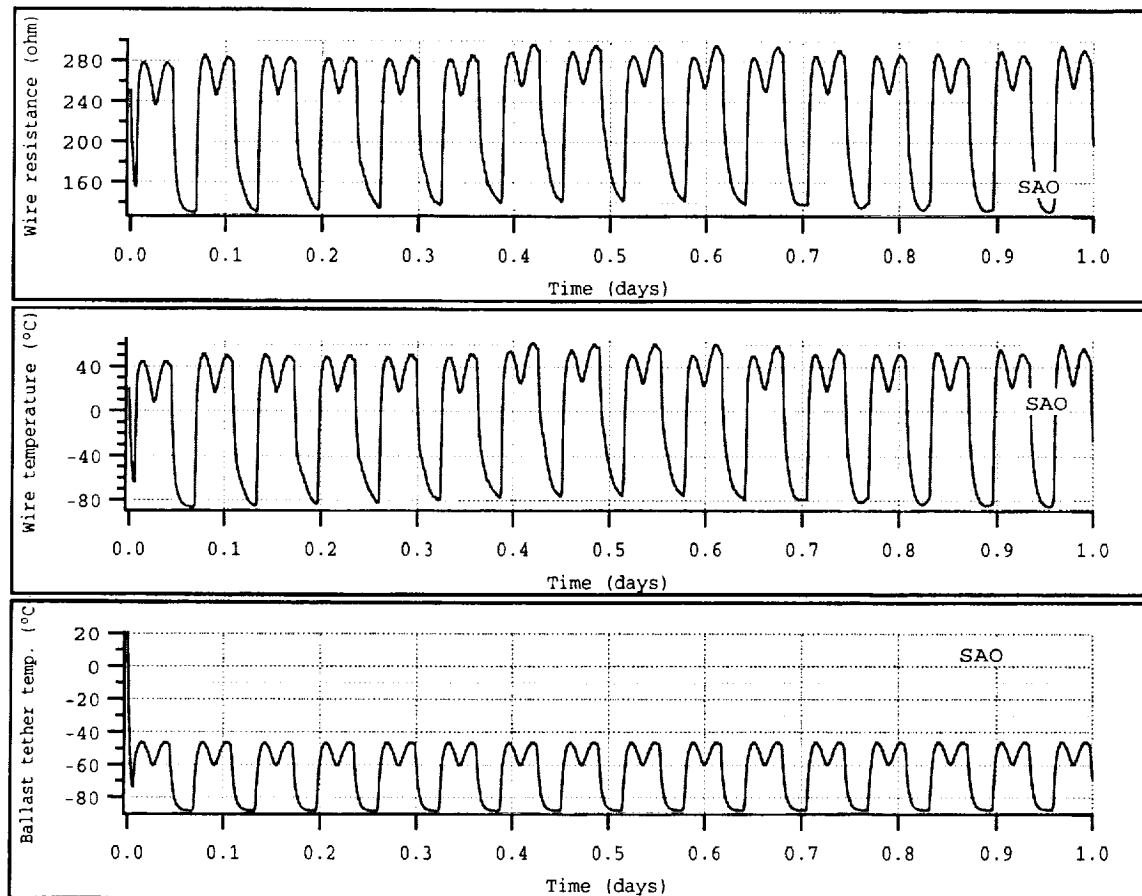


Figure 14 Results for Summer 2002 launch, plasma density twice nominal

ProSEDS 250 ohm@20 C, 360km, double plasma, 00:15:00UT, 25 July 2002

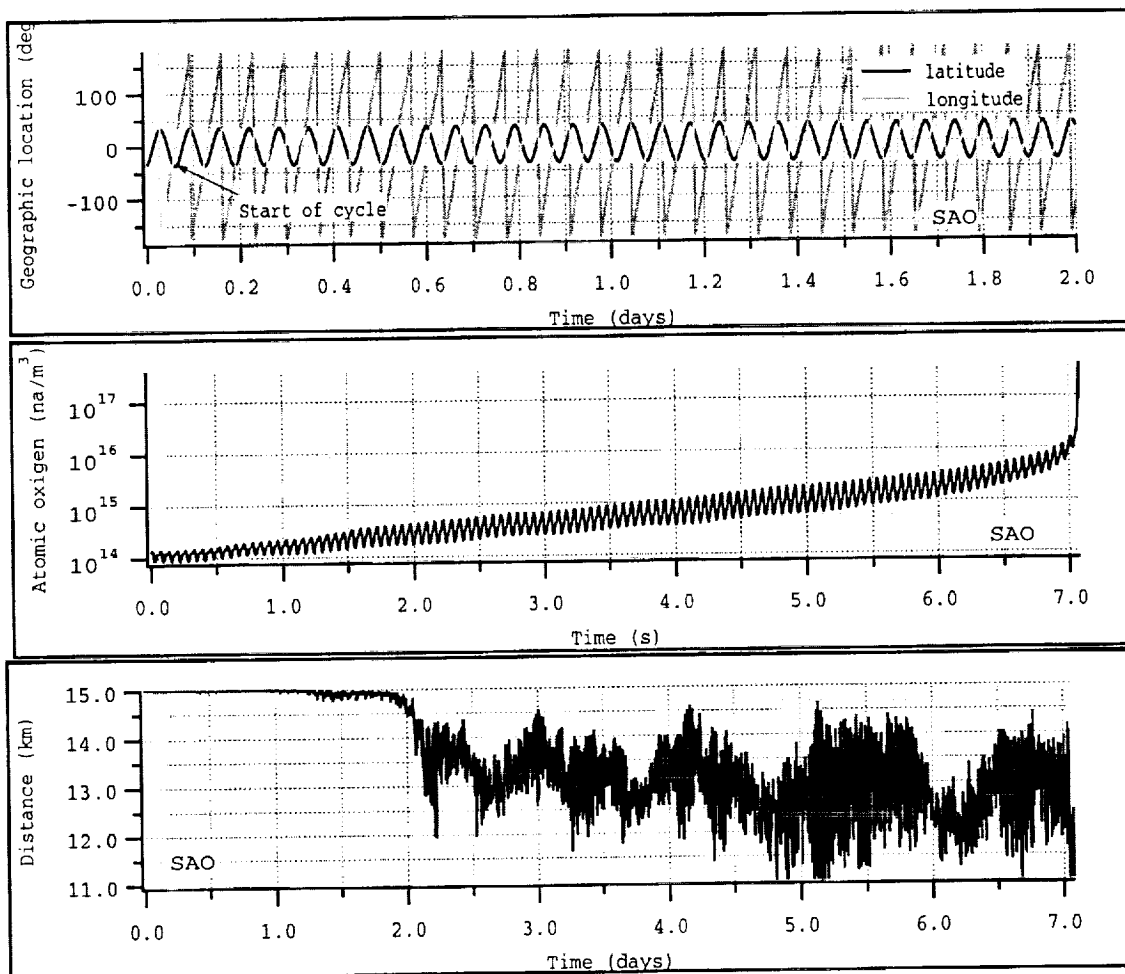


Figure 15 Results for Summer 2002 launch, plasma density twice nominal

1.5 Concluding Remarks

The changes in the operating cycles and most notably the elimination of the open-circuit mode during the 80-s cycles have changed the decay rate and dynamic response of ProSEDS. The present estimates of the orbital decay rate for a launch on July 25th, 2002 are 11 km/day while operating the 60-s cycle (for 5 orbits) and 19 km/day while operating the 80-s cycle during the remainder of the mission but before the neutral drag overpowers the electrodynamic drag. The decay rates estimates are valid with good approximation for any launch date during the Summer of 2002 because the estimated ionospheric and solar indexes that drive the plasma density vary only moderately over the three-month Summer period.

An extreme case with a plasma density twice as high as for nominal solar conditions was run to check the dynamical stability of the system. The decay rate increases only by 20% with respect to the nominal case thanks to the characteristic of the bare-wire anode to adjust to variations of the plasma density. The dynamics of the system remains stable.

2.0 EVALUATION OF POWER DELIVERED BY THE TETHER

2.1 Introduction

The elimination of the open-circuit mode in the 80-s operating cycle changes the amount of electrical energy available to recharge the battery. As a matter of fact, the change in the operating cycle increases the time spent in battery charging mode (i.e., mode 4) from the previous 35 s to 50 s per cycle. Moreover, the value of the tether resistance of the flight tether is lower (250 ohm at 20 °C) than the value of 265 ohm (at 20 °C) utilized in the previous estimates of the current produced by the tether. Consequently, a new estimate of the tether current during battery charging was carried out as shown in the following subsections.

2.2 Numerical Results

The estimate of the tether current produced during battery charging was computed for minimum solar activity conditions predicted for July 2002. The minimum solar conditions, corresponding to a 5% percentile probability, provide a conservative estimate of the tether current (and consequently power) available to recharge the secondary batteries. All other orbital and system parameters are the same of the reference mission described in Section 1.0 of this report. Figure 16 shows the instantaneous tether current during battery charging (mode 4) and the 12-hour running average of the current. The average is computed over the mode-4 period of 50 s and not over the overall cycle of 80 s.

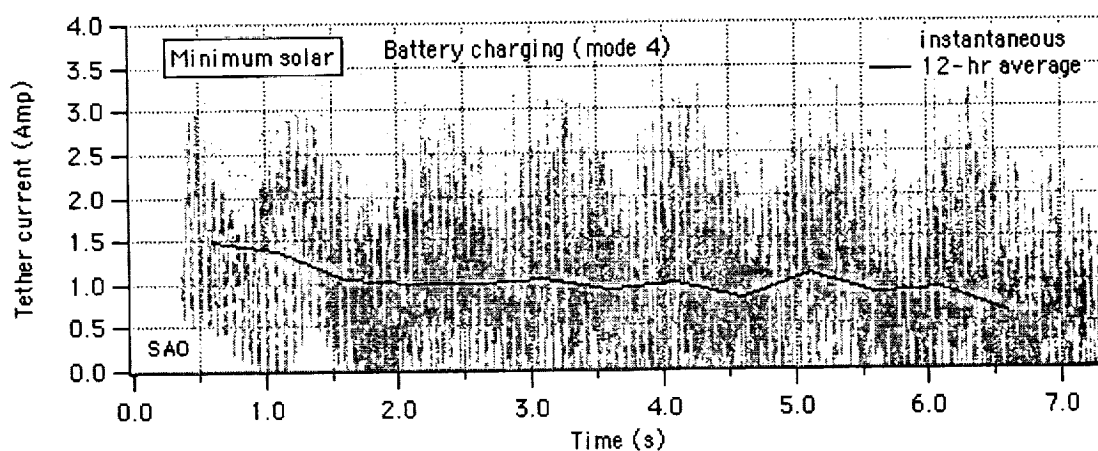


Fig. 16 Tether current during battery charging mode: instant value and 12-hour average

The average value of the current is 1.33 Amp during the first day while the peak value of the current is 3.71 Amp. The corresponding values for nominal solar conditions (the plot is not shown) are 1.42 Amp for the average and 3.85 Amp for the peak value during the first day. The average value of the current decreases by roughly 30% after 1.5 day mostly due to tether dynamics.

Although the average values of the current during battery charging are similar to those computed for earlier launch dates, the net advantage of the new 80-s cycle is that the electrical energy provided by the tether (during normal battery charging operation) is higher because mode-4 is now 50-s long as opposed to 35 s for the older version of the cycle.

2.3 Concluding Remarks

The change in the 80-s operating cycle has improved the power budget for ProSEDS because of the longer time spent in battery-charging mode (mode 4). The estimate of the average current for the first day of operation in battery charging mode is 1.33 Amp for minimum solar conditions with the average computed over the 50-s battery charging mode. The estimated average value for nominal solar conditions is 1.42 Amp. The average values decrease by roughly 30% after 1.5 day due to system dynamics.

The value of the average current is similar to what was computed for the previous launch dates. However, the total electrical energy available for battery charging (during normal battery operation) is better than with the older 80-s cycle because the battery charging mode is now 50-s long as opposed to 35 s.

3.0 UPDATED DEPLOYMENT CONTROL PROFILES AND SIMULATIONS

3.1 Introduction

We recall here that the ProSEDS control law consists of three distinct modes of operations which are activated during the deployment of the three different tether sections. The non-conductive 10-km-long Dyneema tether is deployed according to the SEDS-II feedback-feed-forward control law. During the deployment of the 4.85-km conductive wire, the brake is simply kept at a constant, low value in order to limit the deployment velocity. During the deployment of the 215-m insulated tether section, the brake is commanded to follow a time-based profile to slow down the deployment velocity at the end of the tether.

As explained in details in the Annual Report #1, the control law utilizes a set of control parameters and a reference table that provides the feed forward information to the first portion of the control law. The reference table provides the control law with the nominal deployed length, speed (in terms of turn counts and turn count rate) and brake profiles that the system should follow under ideal conditions. The feedback, then, adjust the nominal fed forwarded brake profile based on the errors of the actual length and speed with respect to the nominal length and speed profiles.

The second and third portions (for the CCOR wire and insulated section deployment) are open-loop control. The second portion is a tension-offset control in which the brake is kept constant at a low value of turns simply for increasing the tether tension and reduce the maximum exit velocity. The wire is coated with a fairly delicate coating that can be rubbed off by excessive friction. Consequently, it is not possible to utilize a feedback control that ramps the brake up and down. The offset value of the brake utilized during this portion is a constant 0.5 brake turn for the flight control law.

In the third portion of the control law, the brake is made to follow an open loop rampup-constant-ramp down profile. This control law acts on the 215-m-long section of the tether with a quick ramp up phase. Because of the absence of a sensor that measure the exit velocity directly in the SEDS hardware, the velocity must be computed numerically from a noisy signal and then filtered to make it usable for a feedback control law. This process is actually used in the first portion of the control law where a delay in the computation of the velocity does not affect the performance of the controller. Due to the short reaction time available for the tether slow down, we opted for an open-loop control during this phase and we shaped the slow down profile in such a way that it is rather

tolerant of changes in the friction characteristics of the tether (see Annual Report #1 for more details).

3.2 Friction model

We rewrite in the following the frictional tension model (derived originally by J. Carroll, see also Ref. ⁷) of the tether and its parameters for the reader's convenience:

$$T = \left(T_0 + I \cdot \rho \cdot \dot{L}^2 \cdot A_{rel}^E \right) \cdot k^{2\pi f n^{effe}} \cdot e^{f|\theta_0 - \theta|} \quad (1)$$

In equation (1), the term in round parenthesis is the frictional model of the tether/deployer. The first exponential function with base k is the model of the brake and the second exponential function with base e is the model of the tether exit guide. The model parameters are:

A_{rel}	$= 1 - A_{sol} \cdot L / L_{fin}$
A_{sol}	$=$ annulus solidity of tether
L	$=$ length of tether deployed
L_{fin}	$=$ final length of tether
B	$= 2\pi f n$ (n is the number of tether turns wrapped around the brake post)
T_0	$=$ minimum tension
ρ	$=$ linear density of tether
I	$=$ inertia multiplier
\dot{L}	$=$ tether exit speed
θ	$=$ tether's exit angle with respect to the local vertical
θ_0	$=$ tether deployment null angle (orientation of the longitudinal axis of deployer with respect to the local vertical)
f	$=$ friction coefficient
n	$=$ number of brake turns
$effe$	$=$ brake effectiveness coefficient
k	$=$ base of the brake power law

The updated values of the friction parameters obtained from the deployment tests on ground of the F-1 tether are as follows:

 Date: 8 January 2002
 From: E.C. Lorenzini (SAO)

Friction Parameters of the F1 flight tether

The reference values of the tension parameters for the ProSEDS tension model are as follows. These values are based on the deployment test (room temp.) of the F1 tether.

Flat Dyneema (cleaned)

T_{\min}	= spectra minimum tension	= 18 mN
den	= spectra linear density	= 0.2 kg/km
I	= inertia multiplier	= 2.0
f	= spectra friction coeff	= 0.17
E	= area exponent	= -0.4
effe	= brake effectiveness $\text{Turn}^{\text{effe}}$	= 1.2
AnSol	= annulus solidity	= 0.2 (for $L_F = 10\text{km}$)
k	= base of braking power law	= 1.7

Wire (CCOR)

T_{\min}	= wire minimum tension	= 75 mN
den	= wire linear density	= 1.935 kg/km
I	= inertia multiplier	= 1.7
f	= friction coeff	= 0.19
E	= area exponent	= -0.65
effe	= brake effectiveness $\text{Turn}^{\text{effe}}$	= 1.2
AnSol	= annulus solidity	= 0.947 (from 1.25km -> 6.25km)
k	= base of braking power law	= 2.72 (= e)

Insulated (Kevlar overbraided)

T_{\min}	= insulated minimum tension	= 300 mN
den	= insulated linear density	= 3.176 kg/km
f	= friction coeff	= 0.22
I	= inertia multiplier	= 1.7
E	= area exponent	= -0.65
effe	= brake effectiveness Turn ^{effe}	= 0.9
AnSol	= annulus solidity	= 0.947
k	= base of braking power law	= 2.72 (= e)

Subsequent tests of the F-1 run in hot and cold conditions validated most of the values of the friction parameters with the exception of the minimum tether tension which is more sensitive to temperature variations and even more importantly to the amount of residual sizing agent in the non-conductive tether (level of cleanliness). The flight tethers have all been cleaned in order to provide values of the minimum tension below 20 mN. However, the control law is tested (as shown later on) also for much higher values of the minimum tension. The typical range of variation of the non-conductive tether minimum tension is assumed conservatively to be in the range 5mN-30mN which are the limit values measured during the deployment tests of the many tethers developed for ProSEDS (and not just the F-1).

The friction parameters of the whole tether (with the three different sections) are utilized to derive the reference table, that is, the reference deployment profile and a brake profile for the whole tether. The brake actuation is then adjusted by the feedback control law during the deployment of 10-km Dyneema portion while the reference brake profile is followed (without adjustments) during the wire and insulated portions of the tether.

3.3 Flight reference table

Several new reference tables were derived for the deployment control law as tether friction data became available during the year from the deployment tests and spooling data from Tether Applications, Inc. We will not describe here all the new updates but rather concentrate on the flight reference profile (Reference #78).

The process for deriving the reference profile is an optimization process that aims at minimizing a cost function which encapsulates the departure of the final dynamic state from the desired state. The desired final state at the end of deployment is for the system to be aligned and swing less with respect to the local vertical with a residual longitudinal velocity greater than 3 m/s before the beginning of the insulated portion of the wire (last 215 m of tether). The residual velocity is then reduced by a final activation of the brake immediately after the exiting of the insulated wire is sensed. The process for deriving the reference profile is described in more detail in the Annual Report #2.

The flight reference table was derived based on the friction data of the F-1 tether deployment test at room temperature and for a minimum tether tension equal to 20 mN. This minimum tension is slightly higher than the 18 mN measured in that deployment test but the 20 mN value provided a reference profile with better features (e.g., smoothness of the deployment velocity and progressive ramping up of the brake) than what could be obtained with the 18 mN value. The friction data from the room temperature test were preferred to the hot and cold test data because the deployer will be close to room temperature at the start of deployment.

The most recent parameters adopted for deriving the flight reference profiles are as follows

Orbital and ejection parameters

Orbit: 360x360 km

Orbital inclination: 36 deg

Ejection velocity = 2.74 m/s

Ejection angle = 5 deg (forward of LV with an upward deployment)

System parameters

Satellite mass = 21.4 kg

Delta-II Mass = 994 kg

Tether lengths: 10132 m Dyneema, 4865 m CCOR and 215-m insulated

Tether length is then converted to tether turns (and velocity to turn rate) which are the variable utilized by the control law. Consequently, two tethers appear very similar to the control law if the number of turns of the three segments are about the same. The following files (supplied by J. Carroll, Tether Applications, Inc.) provide the spooling data for the F-2 and F-3 tethers, respectively

F-2 flight tether spooling

Tether Applications, Inc.

Here are the quadratic equations for the Kevlar+Dyneema, CCOR, and overbraided insulated wire. The values are derived from the turns and estimated as-deployed lengths at various points in the winding, including the estimated effects of Dyneema creep during bakeout, and the temperature and tension differences between winding and deployed conditions. (The deployed tension is assumed to be ~1.3 newtons.) The "L" in meters and "T" (in core turns) for each segment start at zero when that segment starts deploying.

Quadratic length formula for PROSED19 winding of F-2 tether:

Noncond: 10132 meters; 14733 turns; $L = 0.72822 * T - 2.75E-6 * Sqr(T)$

C-COR: 4865 meters; 11037 turns; $L = 0.64497 * T - 18.5E-6 * Sqr(T)$

Insul: 215 meters; 1108 turns; $L = 0.2339 * T - 36E-6 * Sqr(T)$.

The F-2 non-conductive tether is 5 turns & 92 meters longer than F-1. The F-2 wire is 138 turns shorter but 12 meters longer than F-1. Most of these differences are due to the increased bulk of the longer overbraid on F-2, and the fact that we needed about the same wire length but the same # of Dyneema turns.

Meters	Turn#	Transition
0	0	Outer Kevlar tie-down
20	28	End of Kevlar leader (start of Dyneema)
5562	7872	Near the middle of the Dyneema
10132	14733	Start of wire (end of Dyneema)
12705	19328	Near the middle of the wire
14334	23384	Parallel/criss-cross winding transition
14997	25770	Start of overbraided insulated wire
15012	25835	Brake turn (second of two to deploy)
15212	26878	Termination pin at base of core

F-2 cross-straps and key transitions (m) from inner termination pin:

Meters	CoreTurn	Feature
0	0	Termination pin at base of deployer
200	1043	Brake enable sensor hole
215	1108	End of overbraided insulated length.
257	1287	1 (inboard cross-strap; rest are spaced 321m apart)
578	2507	2
900	3559	3
1221	4484	4
1542	5331	5
1863	6119	6
2184	6853	7
2505	7547	8
2826	8206	9
3147	8835	10
3469	9438	11
3790	10015	12
4111	10572	13
4432	11110	14
4753	11631	15
5074	12136	16 (outboard cross-strap)
5080	12145	End of wire (7 wires tuck into core, 1" apart)

F-3 flight tether spooling data

End-to-End Description of Flight Winding of F-3 (PROSED21)

Joe Carroll
Tether Applications, Inc.
Winding dates: March 18-19, 2002
Post-wind handling finished March 21, 2002

Notes on winding:

F-3 quadratic length formulas (winding PROSED21):
Non-conduct: 10167 meters; 14730 turns; $L = 0.73029 \cdot T - 2.72E-6 \cdot \text{Sqr}(T)$
C-COR wire: 4870 meters; 11042 turns; $L = 0.64642 \cdot T - 18.6E-6 \cdot \text{Sqr}(T)$
Insul wire: 214 meters; 1103 turns; $L = 0.2337 \cdot T - 36E-6 \cdot \text{Sqr}(T)$.

For comparison, here are the formulas for F-2 and F-1:

F-2 quadratic length formulas (winding PROSED19):
Non-conduct: 10132 meters; 14733 turns; $L = 0.72822 \cdot T - 2.75E-6 \cdot \text{Sqr}(T)$
C-COR wire: 4865 meters; 11037 turns; $L = 0.64497 \cdot T - 18.5E-6 \cdot \text{Sqr}(T)$
Insul wire: 215 meters; 1108 turns; $L = 0.2339 \cdot T - 36E-6 \cdot \text{Sqr}(T)$.

F-1 quadratic length formulas (for first winding, PROSED15):
Non-conduct: 10040 meters; 14728 turns; $L = 0.7215 \cdot T - 2.70E-6 \cdot \text{Sqr}(T)$
C-COR wire: 4894 meters; 11350 turns; $L = 0.6378 \cdot T - 18.2E-6 \cdot \text{Sqr}(T)$
Insul wire: 174 meters; 933 turns; $L = 0.2201 \cdot T - 36E-6 \cdot \text{Sqr}(T)$.

Tether mass/length:
Kevlar: 2.10g/m
Dyneema: 0.150g/m
CCOR: 1.92g/m
InsWire: 3.25g/m

Transition locations for F-3 (PROSED21):

As wound:		As deployed:		Transition
MetW	Core	Meters	Turn#	
30917	26875	0	0	Outer Kevlar tie-down
30878	26849	19	26	End of Kevlar leader (start of Dyneema)
19596	19008	5577	7867	Stop mid-Dyneema (0.2% longer in orbit)
10278	12145	10167	14730	Start of wire (end of Dyneema)
5072	7556	12741	19319	Stop mid-wire (wire=0.07% shorter)
1777	3497	14371	23378	Parallel/criss-cross transition
430	1103	15037	25772	End of overbraid wrap-splice
402	1044	15051	25831	Brake turn (second of two to deploy)
0	0	15251	26875	Termination pin at base of core

Turn differences of F-2 (PROSED19) and F-1 (PROSED15 & PROSED18) from F-3:

F-2	F-1#1	F-1#3	Transition
+3	-2	+76	Start of wire (end of Dyneema)
+6	-233	-154	Parallel/criss-cross transition
-2	+306	+453	End of overbraid wrap-splice
+4	+102	+228	Brake turn (second of two to deploy)
+3	+136	+272	Termination pin at base of core

Basis of length estimates:

Estimated as-deployed length per turn of TAI metwheel (491.066mm/turn w/o tether) 496.5 mm for insulated overbraided tether & 20m Kevlar leader (same as as-wound) 494.5 mm for C-COR-coated conductive tether (this is 0.07% shorter than as-wound) 492.6 mm for flat 13x100 Dyneema braid (this is 0.2% longer than as-wound)

Winding temperature range: ~21-23C

Winding tension (lengths were measured at these tensions):

13-16 newtons for parallel winding

12, 10.5, 9, 7.5, and 10 newtons for CC patterns #1-5.

Explanation of adjustments from as-wound to as-deployed conditions:
Assume Dyneema creep during bakeout reduces its tension to as-deployed tension.

Assume Kevlar has equilibrium post-deployment tension of ~1.3 newtons
Modulus of long segments (C-COR and Dyneema) is ~12000-15000 newtons.
Assume Dyneema and CCOR are 225K and 300K in orbit; CTEs are -28ppm/K and 0ppm/K. Thus Dyneema should be ~0.2% longer; CCOR ~0.07% shorter, deployed vs. wound.

F-3 Cross-strap locations (from start of winding):

MetWhl	CoreTurn	Meters	Gap
530W	1311.1C	262	262
1179W	2524.4C	584	321
1828W	3572.4C	905	321
2477W	4495.5C	1226	321
3127W	5343.7C	1547	322
3777W	6131.4C	1869	321
4426W	6866.1C	2190	321
5076W	7559.4C	2511	321
5725W	8217.9C	2832	321
6373W	8846.7C	3153	321
7023W	9447.5C	3474	321
7672W	10024.0C	3795	321
8322W	10578.9C	4116	321
8970W	11115.3C	4437	321
9619W	11633.7C	4758	321
10267W	12136.6C	5078	320

The differences in turns of the F-2 from the F-3 are less than 6 turns which makes them almost perfectly alike to the control law. The reference profile (Ref. #78) works equally well for the F-2 and F-3 flight tethers. This reference profile, shown in Figure 17, has several good features as follows: (a) the exit velocity changes smoothly during the Dyneema deployment and it does not deep down to low values; (b) the brake increases monotonously from zero to its maximum value; and (c) the libration angle is very close to zero at the end of deployment (for reference conditions). This reference profile when combined with the control law provides a final libration amplitude which is quite insensitive to variation of the Dyneema minimum tension and other friction parameters as it will be shown later on. The reference table for Ref. #78 is tabulated in Appendix A.

Reference Profile #78

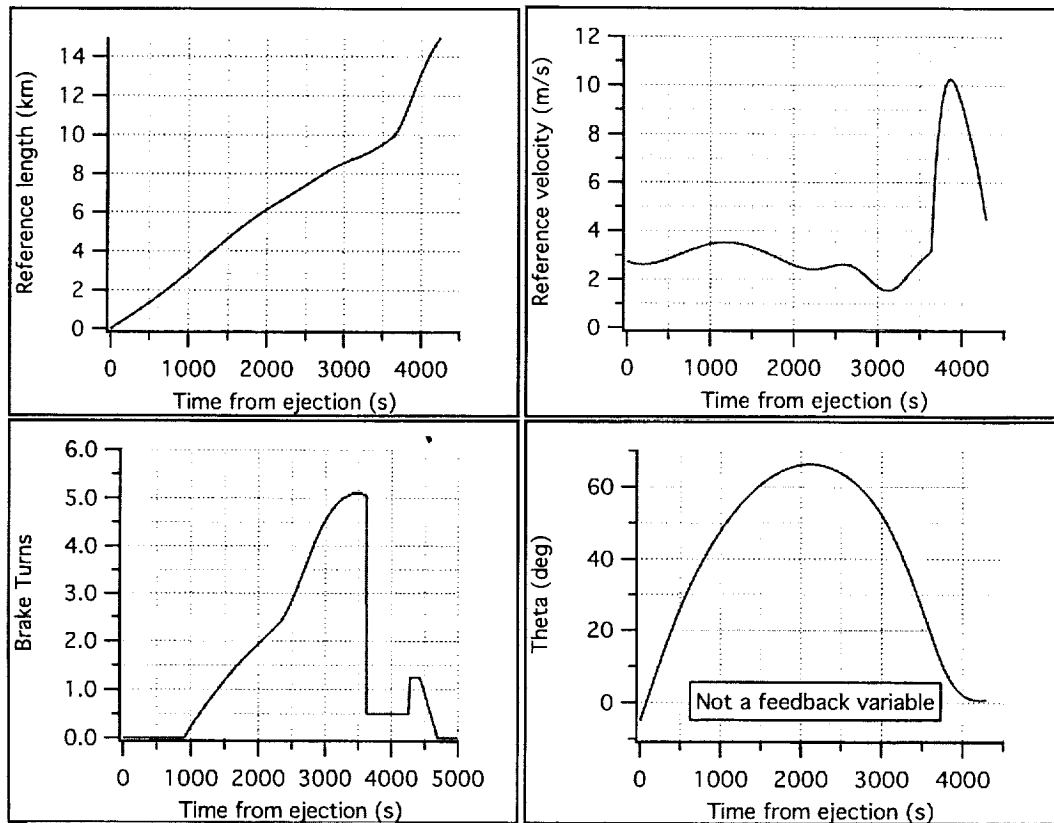


Figure 17 Control law Reference Profile #78

3.4 Flight control law parameters

The control law not only provides the logic for controlling deployment under perfect functionality of the sensors. It also has a set of backup modes to circumvent or mitigate the effects of possible failures or malfunctions of the deployer sensors. The sensors in question are the two turn counters (Counter-A and Counter-B) which measure the number of tether turns that have been deployed. In standard operation, the output of the two turn counters is combined to produce a software turn count Counter-C which is unaffected by double counts. In case of failure of one of the turn counter, Counter-C is bypassed and the still functioning turn counter is utilized by the sensor logic. However, when only one turn counter is working there is an over count of the number of turns that has to be accounted for by the control law when transitioning from one tether segment to the next. Also, if both turn

counters fail, the control law logic sets the feedback to zero and utilizes exclusively the reference profile to drive deployment (this is one additional advantage of having the feed-forward profile in the control law). Similarly, there are two levels of backup for the actuation of the slow down maneuver that starts at the beginning of the insulated tether portion (last 215 m of tether). The slow down maneuver is activated, in standard operation, by the turn counter. In case of the two turn counters failing, there are two level of backup as follows: the first one is provided by the brake enabler switch which senses the beginning of the insulated wire and the second is provided by time.

The control parameters define the standard operation of the control law and also the activation of the backup modes. The parameters controlling the standard operation are taken from the SEDS-II control set with a few adjustments aimed at improving the robustness of the control law to variations of the friction parameters. The control parameters that define the control modes corresponding to transitions from one tether segment to the next and the parameters that define the backup modes have been added to the original control set of the SEDS-II control law. The complete set of the updated control parameters for Reference #78 are shown in Table 1.

Table 1 Updated control parameters for Reference #78

Values of control parameters for ProSEDS Ref#78 (F2 & F3 tethers). Issued on April 5, 2002; revised on July 23, 2002.

----- CONTROL PARAMETERS (REF. #78) -----			
No.	PARAMETER	VALUE (Units)	Type
1.	c	0.125	Filter coefficient
2.	GTC	0.002 (1/turn)	TurnCount Gain
3.	DZTC	5 (turn)	TurnCount Deadzone
4.	TCELIM	3000 (turn)	Max. TurnCount Error
5.	GTCR	0.4 (s/turn)	TurnCountRate Gain
6.	DZTCR	0.1 (turn/s)	TurnCountRate Deadzone
7.	TCRELIM	5 (turn/s)	Max. TurnCountRate Error
8.	WAILP	3	WrapIncrement UpperLimit
9.	TBD s	65535 (sec)	Time after which BIAS is applied
10.	BIAS	0 (turn)	BrakePost Bias
11.	WACLP	6.5 (turn)	WrapAdjustment UpperLimit
12.	TCBS	18000 (turn)	Turns Count Brake Stop (SEDS-II law)
13.	A1	0.724	Coeff_1 in Variable Gains
14.	A2	2.82E-6	Coeff_2 in Variable Gains
15.	STOPDEPLOY	65535 (sec)	Time for brake ramping up to max. value at end of deployment (SEDS-II law)
16.	TCDUTY	13560 (turn)	End of 50% duty cycle
17.	TURNBRAKE0	14265 (turn)	RampDown brake to WIREBRAKE
18.	WIREBRAKE	0.5 (turn)	BrakeTurns during CCOR deployment
19.	RAMPUP	25835 (turn)	Start of slowdown procedure

20. QUITLAWBACKUP	14400	(turn)	Ramp down brake in case of CounterA or B failure
21. BRSD	1.25	(turn)	Max brake turns during slow down
22. TBD(15)	20	(sec)	Time to rampup brake from WIREBRAKE to BRSD
23. TIMECFAIL	120	(sec)	Time of no update of CounterC to declare the CounterC failed
24. TIMEDUTY	6080*	(sec)	Time-based equivalent of TCDUTY
25. TIMEQUERY	6832*	(sec)	The software starts interrogating the BES if CounterC has failed
26. TIMERAMPNOBES	6894*	(sec)	Time-based start of slowdown procedure if the BES was declared failed

*These values of parameters assume a SMET = 2640 sec at endmass separation (parameters revised on July 23, 2002)

Notes:

BES = brake enable switch
 SW = flight software
 SMET = secondary mission elapsed time

3.5 Sensitivity of control law to friction parameters

Deployment trajectory is mostly influenced by the tether tension profile during the early part of deployment (see Ref. ⁸). The physical explanation for this behavior is that small changes in the tether changes alter the dynamics the most when the external forces (i.e., the gravity gradient) are small, that is, at short tether lengths.

The deployment test data show that the range of variation of most of the friction parameters are smaller than $\pm 20\%$. The minimum tether tensions of the Dyneema and the CCOR wire are the exception. The value of the Dyneema minimum tension in particular changes by a few folds across the many tether samples tested. The CCOR minimum

tension, besides being less variable than the Dyneema, has an almost negligible effect on the libration amplitude at the end of deployment.

The minimum tension of the ProSEDS Dyneema tether (which dominates the final state at the end of deployment) has already been measured in deployment ground tests under different temperatures to vary between 5mN and 30 mN for all the tether samples tested with a smaller range of variation for the F-1 tether. Consequently, the control law must provide a residual libration at the end of deployment of less than 20° (as specified by the mission requirements) within the measured range of variability of the minimum tension.

The control law with Ref. #78 can tolerate without a significant decay in performance a value of the non-conductive tether minimum tension between 5 mN and 30 mN. For $30 \text{ mN} < T_0 < 60 \text{ mN}$, the libration at end of deployment increases above 10° but still below 20° . For $T_0 \geq 80 \text{ mN}$, the deployment stops at a distance of about 500 m because of excessive friction and without any role being played by the control law. The critical value of 80 mN for the minimum tension is determined by the ejection velocity which with the present ejection system is equal to 2.74 m/s.

Figure 18-20 show details of the deployment dynamics for values of the minimum Dyneema tension for $T_0 = 5 \text{ mN}$, 10 mN , and 20 mN (reference value), respectively. Figure 21 shows the effect on the control law and deployment dynamics of a noisy tether tension on the deployment dynamics (for $T_0 = 20 \text{ mN}$). A $\pm 50\%$ white noise has been added to the tether tension. The figure shows that the control law is capable of handling the high noise level with ease. The brake actuation is still smooth and the deployment dynamics is negligibly affected by the noise. The final libration amplitude is unaffected by the white noise.

Ref#78, $T_{min} = 5\text{mN}/150\text{mN}$, $\Delta V = 2.74\text{ m/s}$, Brake 1.25/20s

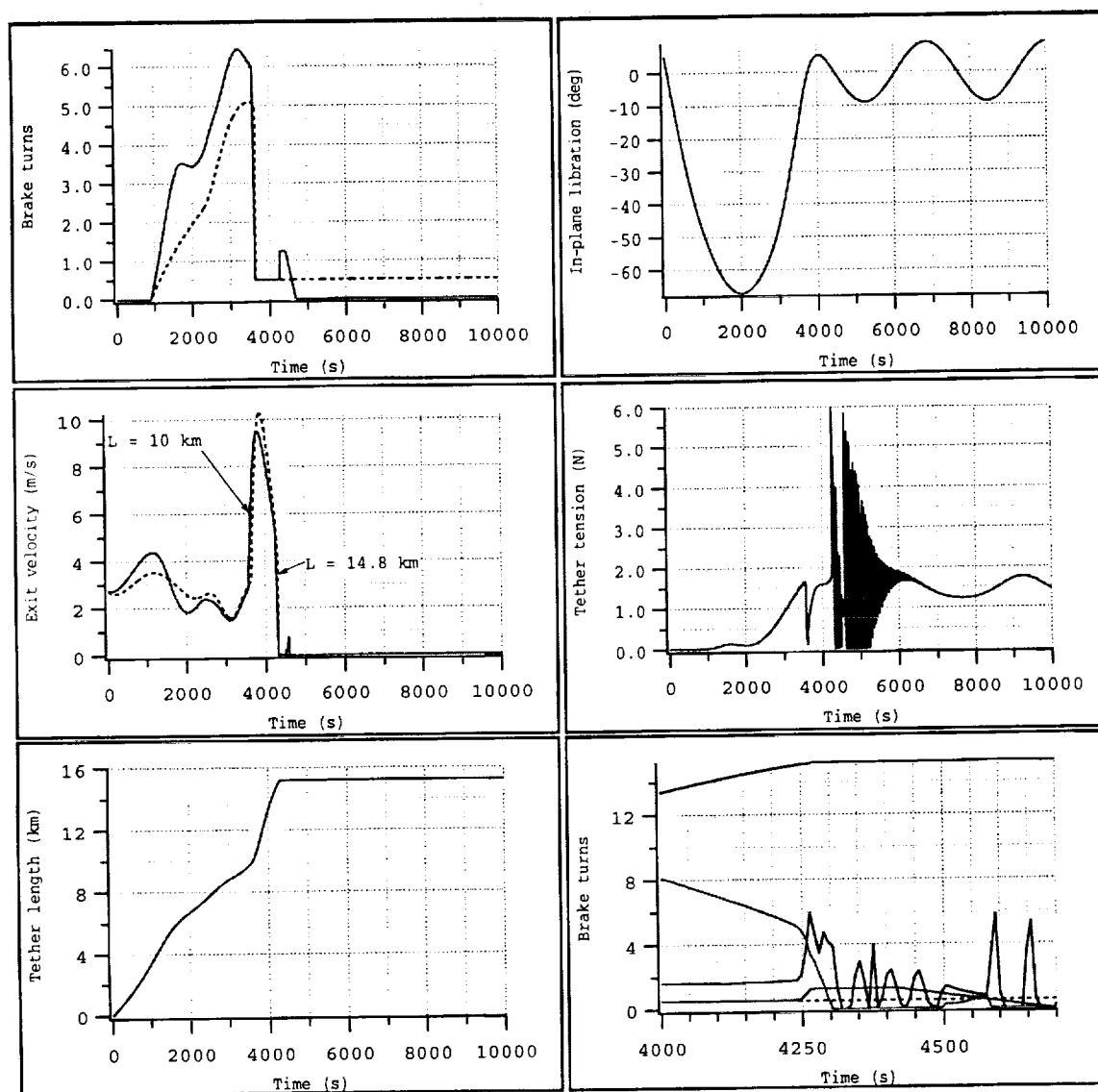


Figure 18 Deployment dynamics for Ref#78 and $T_0 = 5\text{ mN}$

Ref#78, $T_{min} = 10\text{mN}/150\text{mN}$, $\Delta V = 2.74\text{ m/s}$, Brake 1.25/20s

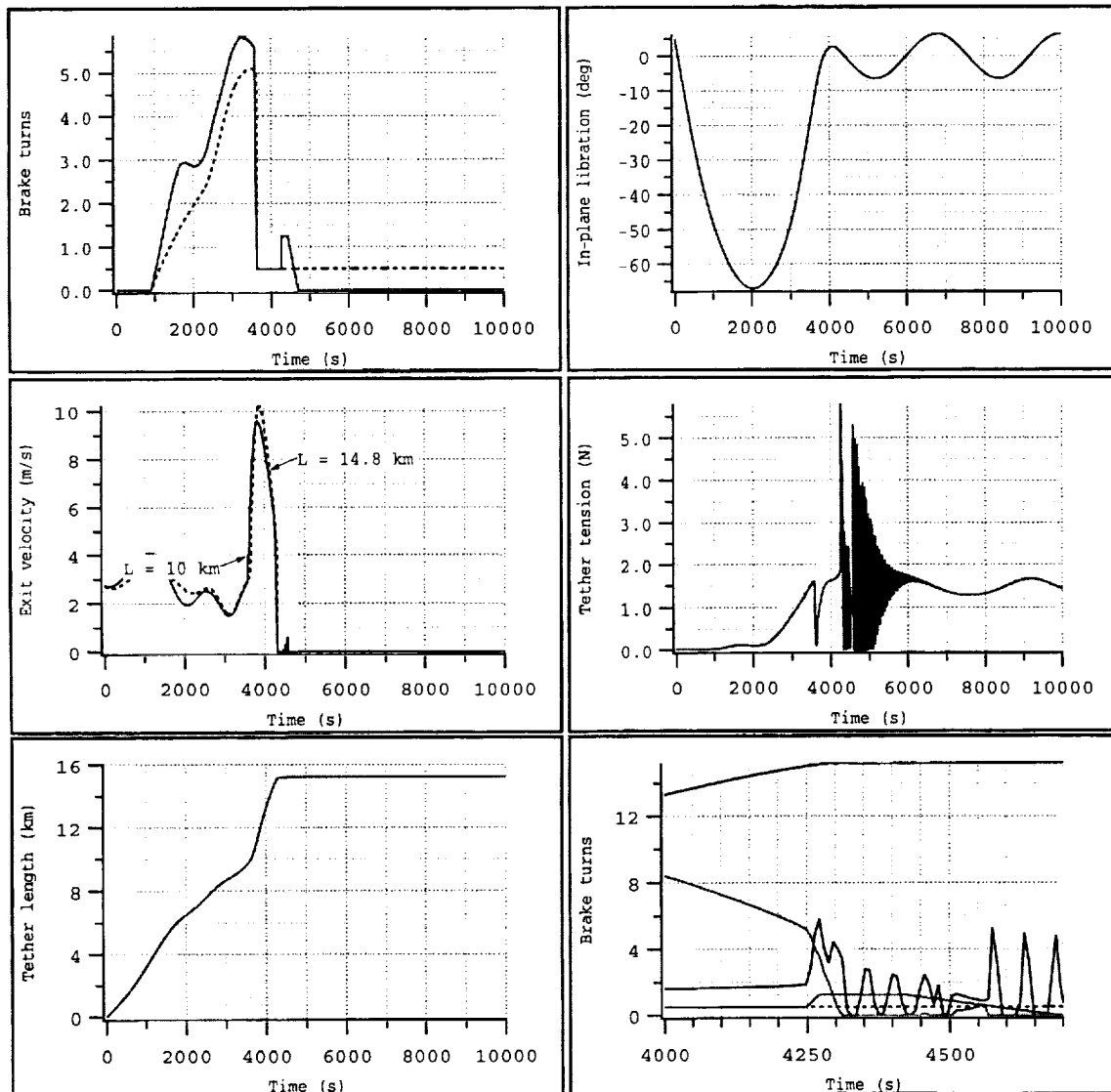


Figure 19 Deployment dynamics for Ref#78 and $T_0 = 10\text{ mN}$

Ref#78, $T_{min} = 20\text{mN}/150\text{mN}$, $\Delta V = 2.74\text{ m/s}$, Brake 1.25/20s

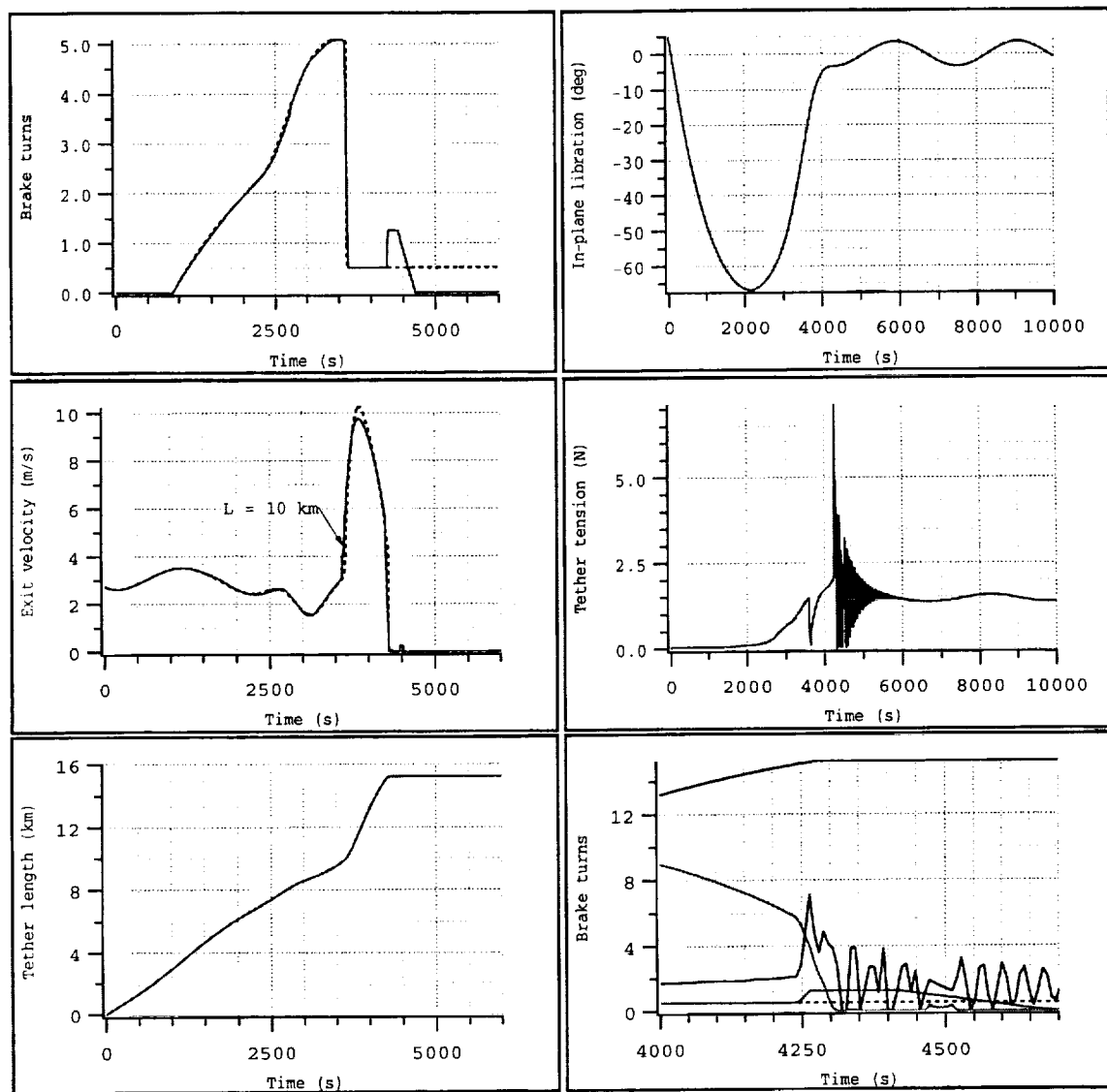


Figure 20 Deployment dynamics for Ref#78 and $T_0 = 20\text{ mN}$ (reference)

Ref#78, $T_{min} = 20\text{mN}/150\text{mN}$, $\Delta V = 2.74\text{ m/s}$, $\pm 50\%$ White Noise

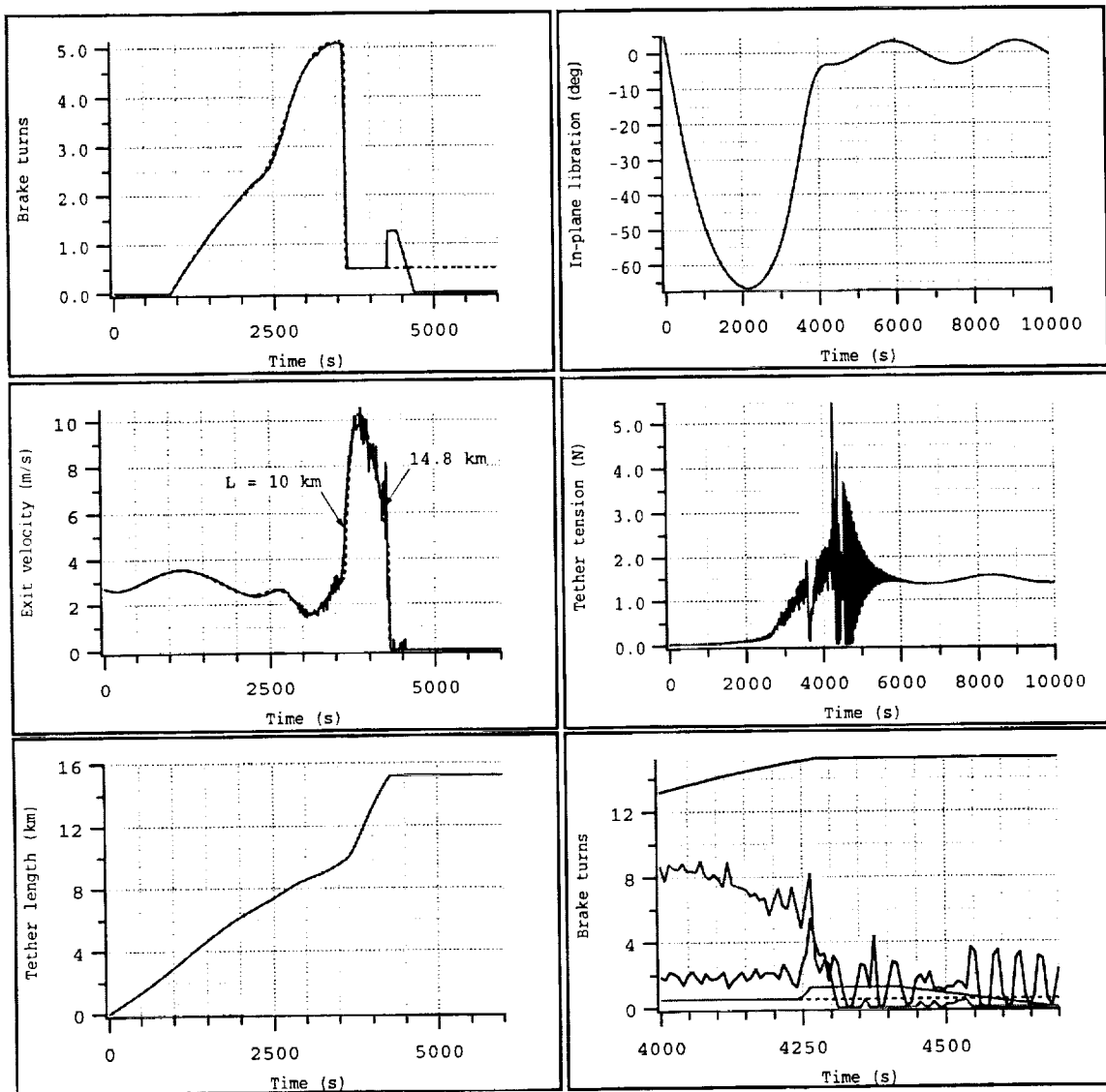


Figure 21 Deployment dynamics for $T_0 = 20\text{ mN}$ with $\pm 50\%$ *tension white noise*

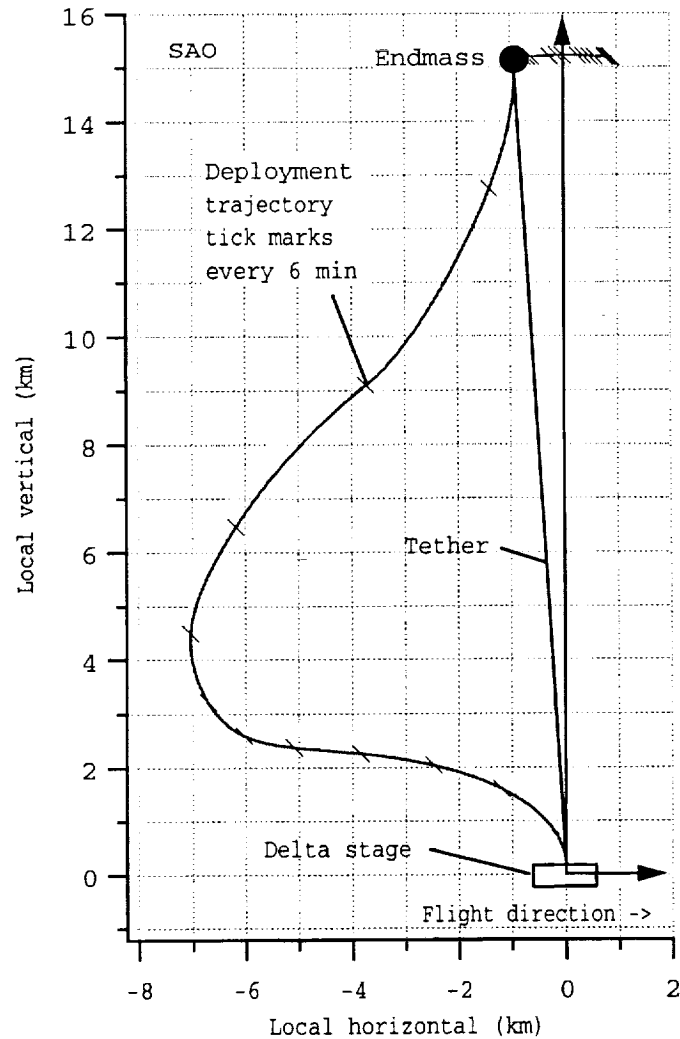


Figure 22 Deployment trajectory of the endmass with respect to the Delta stage

Figure 22 depicts the deployment trajectory of the endmass with respect to the Delta stage for the reference case of $T_0 = 20$ mN. The tick marks along the trajectory are every 6 minutes and the CCOR wire starts deploying at about the point where the tick mark caption is pointing. Figure 23 shows the amplitude of the residual libration at the end of deployment vs. the minimum tension T_0 of the Dyneema tether for Ref. #78. The figure also shows the libration amplitude without deployment control and the representative points of the SEDS-I and SEDS-II missions. The final libration amplitude is sensitive to the Dyneema tether T_0 and it is quite insensitive to the value of the wire minimum tension T_{wire} . Values of T_{wire} of 50-300 mN have been explored with very good deployment dynamics. Values as high as 500 mN are tolerable for the minimum tension of the wire.

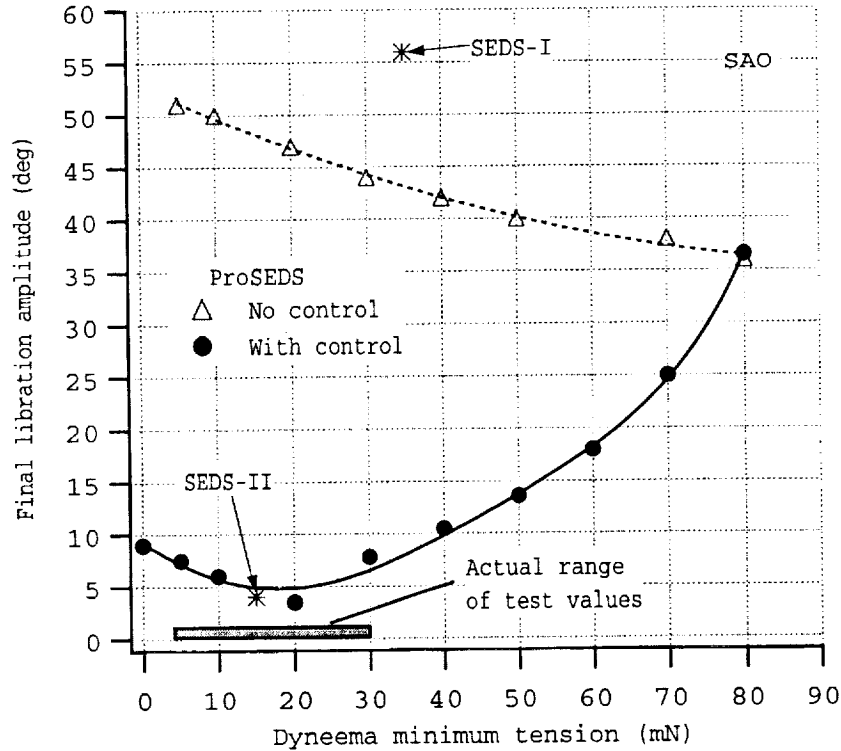


Figure 23 Final libration amplitude vs. T_0 with control (Ref. #78) and without control

3.6 Concluding remarks

The deployment control law in combination with Reference Profile #78 is robust with respect to changes of the most influential and uncertain friction parameters. A number of backup modes have been built into the control logic to circumvent (or mitigate) the effects of the possible failure of one (or two) turn counters. The control law meets the requirement of a final libration smaller than 20° over the measured values of the friction parameters with a positive safety margin.

4.0 ANALYSIS/ESTIMATION OF DEPLOYMENT FLIGHT DATA

4.1 Introduction

The performance of the deployment control law in terms of final libration (and other dynamic variables) can be assessed from the single data stream of the turn counter. In fact, from the (in-plane) libration equation it is possible to see that in the absence of strong external forces (other than gravity gradient forces) the libration state of the system can be extracted from the knowledge of the tether length and speed profiles. Since deployment takes place almost exclusively on the orbital plane, knowledge of the in-plane angle define the libration state of the system.

It is possible to construct an observer of the system libration based on the deployed tether length and exit speed. In the actual case, the only available information is the turn counter which provides the number of deployed tether turns. The tether turns must be first converted into tether length by utilizing the spooling relationship. The length data must be filtered with a low-pass filter before computing the exit speed because any small jump in tether length over a short time period will result in a big jump of tether rate when the speed is computed by numerical derivation.

Finally, the smoothed length and speed can be used as input to the deployment observer in order to compute tether libration and consequently reconstruct the deployment trajectory of the endmass and estimate the libration amplitude after the end of deployment when the attitude of the endmass has stabilized.

An alternative way to the deployment state estimation is to utilize position estimates from the GPS receivers on board the endmass and the Delta and derive the relative dynamics through differences of simultaneous position data. The GPS-method, however, is predicated on having the two signals available from the very beginning of deployment when the endmass is tumbling and prone to losing the signal lock. The GPS method, which will be implemented later on, could be utilized more reliably to backup the estimate of the libration amplitude at the end of deployment.

4.2 Numerical results

In the following we will show results from the deployment observer (i.e., based on the turn counter estimation method). We take a noisy string of turn counter data from the deployment simulation shown in Fig. 21 (with $T_0 = 20$ mN and heavy white noise) and we prove that the deployment trajectory can be reconstructed and the amplitude of the final libration accurately evaluated by means of the process described previously.

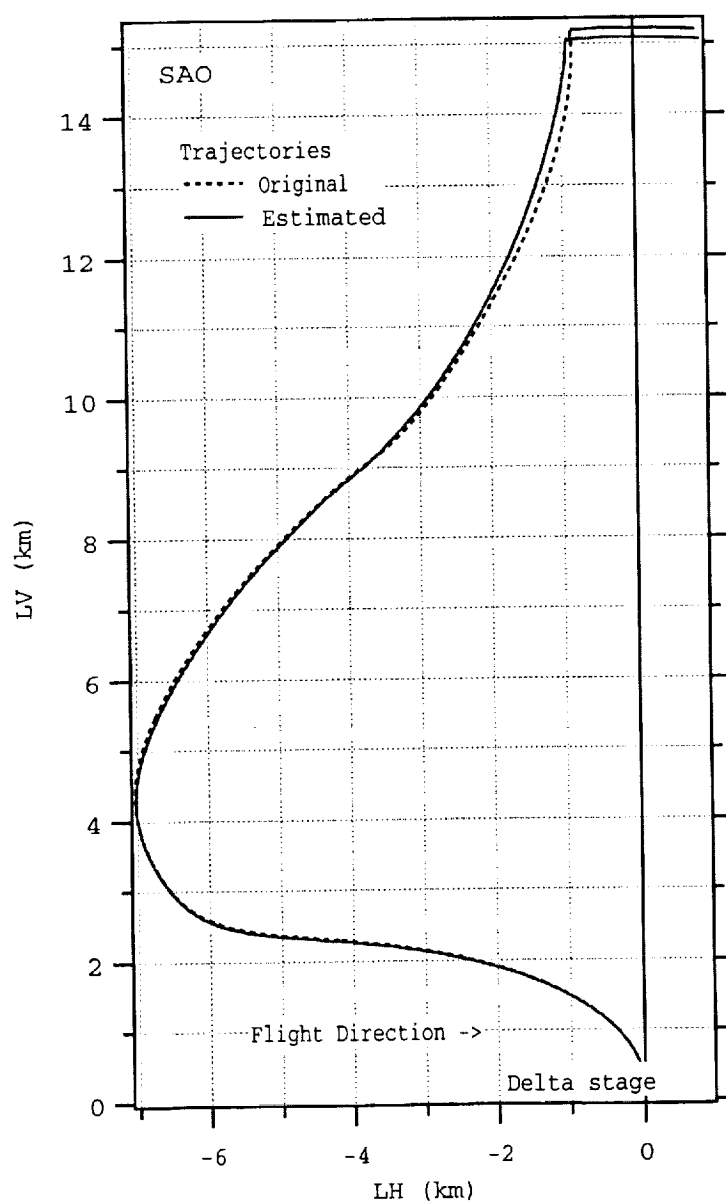


Figure 24 Deployment trajectory of endmass: estimated from noisy turn counter data (solid line); and original data (dotted line)

Figure 24 shows the deployment trajectory of the endmass with respect to the Delta stage estimated from noisy turn counter data (for $T_0 = 20$ mN) and the original trajectory computed from the simulated data shown in Fig. 21. Clearly, the estimation software is capable of extracting the deployment trajectory from noisy turn counter data and of estimating accurately the libration amplitude at the end of deployment. This estimation software was also installed on the computer at NASA MSFC and it was run successfully twice during the mission operation simulations at the EDAC.

4.3 Concluding remarks

The estimation technique based on the data string provided by the turn counter is able to reconstruct the deployment trajectory and provide an accurate estimate of the amplitude of the libration at the end of deployment starting from noisy data. The advantage of this method is that it is based on one string of data that is readily available throughout deployment. The GPS data from both the Delta stage and the endmass can also be utilized to check the estimate of the libration after the end of deployment.

APPENDIX A

Reference Table for ProSEDS deployment control law (Ref#78, flight). For completeness, this file includes data of tether length and tether exit velocity

Date: April 4, 2002

Author: E.C. Lorenzini (SAO)

Support File for ProSEDS Reference #78.

Time (s)	Length (m)	Speed (m/s)	Turn (turn)	Turnrate (turn/s)	Brake (turn)
0	0.5	2.74	1	3.752	0
8	22.378	2.73	31	3.739	0
16	44.173	2.719	61	3.726	0
24	65.889	2.71	90	3.714	0
32	87.53	2.701	120	3.703	0
40	109.101	2.692	150	3.692	0
48	130.605	2.684	179	3.681	0
56	152.044	2.676	208	3.672	0
64	173.424	2.669	238	3.663	0
72	194.749	2.662	267	3.654	0
80	216.021	2.656	296	3.647	0
88	237.245	2.65	325	3.64	0
96	258.424	2.645	354	3.633	0
104	279.561	2.64	384	3.627	0
112	300.662	2.635	413	3.622	0
120	321.729	2.631	441	3.618	0
128	342.765	2.628	470	3.614	0
136	363.775	2.625	499	3.61	0
144	384.761	2.622	528	3.608	0
152	405.728	2.62	557	3.605	0
160	426.679	2.618	586	3.604	0
168	447.617	2.617	615	3.603	0
176	468.545	2.616	643	3.602	0
184	489.467	2.615	672	3.602	0
192	510.386	2.615	701	3.603	0
200	531.306	2.615	730	3.604	0
208	552.229	2.616	759	3.606	0
216	573.159	2.617	788	3.609	0
224	594.098	2.618	817	3.611	0
232	615.05	2.62	845	3.615	0
240	636.019	2.622	874	3.619	0
248	657.005	2.625	903	3.623	0
256	678.014	2.628	932	3.628	0
264	699.046	2.631	961	3.633	0
272	720.106	2.634	990	3.639	0
280	741.196	2.638	1020	3.645	0
288	762.318	2.642	1049	3.652	0
296	783.475	2.647	1078	3.659	0
304	804.67	2.652	1107	3.667	0
312	825.904	2.657	1137	3.675	0

SAO Annual Report #3, NASA Grant NAG8-1605

320	847.182	2.662	1166	3.684	0
328	868.504	2.668	1196	3.692	0
336	889.873	2.674	1225	3.702	0
344	911.291	2.681	1255	3.711	0
352	932.76	2.687	1285	3.721	0
360	954.284	2.694	1314	3.732	0
368	975.863	2.701	1344	3.743	0
376	997.499	2.708	1374	3.754	0
384	1019.194	2.716	1404	3.765	0
392	1040.951	2.724	1435	3.777	0
400	1062.771	2.731	1465	3.789	0
408	1084.655	2.74	1495	3.801	0
416	1106.606	2.748	1526	3.814	0
424	1128.625	2.757	1556	3.827	0
432	1150.713	2.765	1587	3.84	0
440	1172.872	2.774	1618	3.853	0
448	1195.103	2.783	1649	3.867	0
456	1217.408	2.793	1680	3.881	0
464	1239.787	2.802	1711	3.895	0
472	1262.242	2.812	1742	3.909	0
480	1284.775	2.821	1773	3.924	0
488	1307.386	2.831	1805	3.939	0
496	1330.076	2.841	1836	3.954	0
504	1352.846	2.851	1868	3.969	0
512	1375.697	2.862	1900	3.984	0
520	1398.631	2.872	1932	4	0
528	1421.646	2.882	1964	4.015	0
536	1444.746	2.893	1996	4.031	0
544	1467.929	2.903	2028	4.047	0
552	1491.196	2.914	2061	4.062	0
560	1514.549	2.924	2093	4.079	0
568	1537.988	2.935	2126	4.095	0
576	1561.513	2.946	2159	4.111	0
584	1585.124	2.957	2192	4.127	0
592	1608.822	2.968	2225	4.143	0
600	1632.607	2.979	2258	4.16	0
608	1656.48	2.99	2291	4.176	0
616	1680.44	3	2325	4.193	0
624	1704.488	3.011	2358	4.209	0
632	1728.623	3.022	2392	4.226	0
640	1752.846	3.033	2426	4.242	0
648	1777.157	3.044	2460	4.259	0
656	1801.556	3.055	2494	4.275	0
664	1826.042	3.066	2528	4.292	0
672	1850.615	3.077	2563	4.309	0
680	1875.276	3.088	2597	4.325	0
688	1900.024	3.099	2632	4.342	0
696	1924.859	3.11	2667	4.358	0
704	1949.78	3.121	2702	4.374	0
712	1974.787	3.131	2737	4.391	0
720	1999.88	3.142	2772	4.407	0
728	2025.058	3.153	2807	4.423	0
736	2050.321	3.163	2843	4.44	0
744	2075.669	3.174	2878	4.456	0
752	2101.1	3.184	2914	4.472	0
760	2126.615	3.194	2950	4.487	0
768	2152.212	3.205	2986	4.503	0
776	2177.891	3.215	3022	4.519	0

SAO Annual Report #3, NASA Grant NAG8-1605

784	2203.652	3.225	3058	4.535	0
792	2229.493	3.235	3094	4.55	0
800	2255.415	3.245	3131	4.566	0
808	2281.416	3.255	3168	4.581	0
816	2307.495	3.265	3204	4.596	0
824	2333.652	3.274	3241	4.611	0
832	2359.886	3.284	3278	4.626	0
840	2386.197	3.293	3315	4.641	0
848	2412.582	3.303	3352	4.655	0
856	2439.042	3.312	3390	4.67	0
864	2465.575	3.321	3427	4.684	0
872	2492.181	3.33	3465	4.698	0
880	2518.859	3.339	3502	4.712	0
888	2545.607	3.348	3540	4.726	0
896	2572.425	3.357	3578	4.74	0
904	2599.312	3.365	3616	4.754	0.004
912	2626.267	3.374	3654	4.767	0.028
920	2653.287	3.382	3692	4.78	0.048
928	2680.372	3.39	3730	4.793	0.067
936	2707.52	3.397	3769	4.805	0.086
944	2734.729	3.405	3807	4.817	0.104
952	2761.997	3.412	3846	4.829	0.123
960	2789.323	3.419	3884	4.841	0.142
968	2816.704	3.426	3923	4.852	0.16
976	2844.14	3.433	3962	4.863	0.179
984	2871.628	3.439	4001	4.874	0.197
992	2899.166	3.445	4040	4.884	0.215
1000	2926.752	3.451	4079	4.894	0.233
1008	2954.384	3.457	4118	4.904	0.251
1016	2982.061	3.462	4158	4.913	0.268
1024	3009.78	3.467	4197	4.922	0.285
1032	3037.54	3.472	4236	4.93	0.303
1040	3065.338	3.477	4276	4.939	0.32
1048	3093.173	3.481	4315	4.946	0.337
1056	3121.042	3.486	4355	4.954	0.353
1064	3148.943	3.49	4395	4.961	0.37
1072	3176.875	3.493	4434	4.968	0.387
1080	3204.836	3.497	4474	4.975	0.403
1088	3232.822	3.5	4514	4.981	0.42
1096	3260.833	3.503	4554	4.986	0.436
1104	3288.866	3.505	4594	4.992	0.452
1112	3316.919	3.508	4634	4.997	0.469
1120	3344.99	3.51	4674	5.001	0.485
1128	3373.076	3.512	4714	5.006	0.501
1136	3401.177	3.513	4754	5.01	0.517
1144	3429.29	3.515	4794	5.013	0.533
1152	3457.412	3.516	4834	5.016	0.549
1160	3485.542	3.517	4874	5.019	0.565
1168	3513.677	3.517	4914	5.022	0.581
1176	3541.816	3.517	4955	5.024	0.597
1184	3569.955	3.517	4995	5.025	0.612
1192	3598.094	3.517	5035	5.027	0.628
1200	3626.23	3.517	5075	5.028	0.644
1208	3654.361	3.516	5115	5.028	0.659
1216	3682.485	3.515	5156	5.028	0.675
1224	3710.6	3.514	5196	5.028	0.69
1232	3738.704	3.512	5236	5.028	0.706
1240	3766.794	3.51	5276	5.027	0.721

SAO Annual Report #3, NASA Grant NAG8-1605

1248	3794.868	3.508	5316	5.025	0.737
1256	3822.926	3.506	5357	5.024	0.752
1264	3850.964	3.503	5397	5.022	0.767
1272	3878.981	3.501	5437	5.019	0.782
1280	3906.974	3.498	5477	5.017	0.798
1288	3934.941	3.494	5517	5.013	0.813
1296	3962.881	3.491	5557	5.01	0.828
1304	3990.791	3.487	5597	5.006	0.843
1312	4018.67	3.483	5637	5.002	0.858
1320	4046.516	3.478	5677	4.997	0.873
1328	4074.326	3.474	5717	4.992	0.888
1336	4102.099	3.469	5757	4.987	0.903
1344	4129.833	3.464	5797	4.981	0.917
1352	4157.525	3.459	5837	4.975	0.932
1360	4185.175	3.453	5877	4.969	0.947
1368	4212.779	3.448	5917	4.962	0.962
1376	4240.337	3.442	5956	4.956	0.976
1384	4267.847	3.436	5996	4.948	0.991
1392	4295.307	3.429	6035	4.94	1.005
1400	4322.714	3.423	6075	4.933	1.02
1408	4350.068	3.416	6114	4.924	1.034
1416	4377.366	3.409	6154	4.916	1.049
1424	4404.607	3.401	6193	4.907	1.063
1432	4431.789	3.394	6232	4.897	1.077
1440	4458.911	3.386	6271	4.888	1.091
1448	4485.971	3.378	6310	4.878	1.105
1456	4512.967	3.371	6349	4.868	1.119
1464	4539.898	3.362	6388	4.858	1.134
1472	4566.763	3.354	6427	4.847	1.148
1480	4593.559	3.345	6466	4.836	1.161
1488	4620.285	3.336	6504	4.825	1.175
1496	4646.941	3.327	6543	4.813	1.189
1504	4673.524	3.318	6581	4.802	1.203
1512	4700.033	3.309	6620	4.79	1.217
1520	4726.468	3.299	6658	4.777	1.23
1528	4752.825	3.29	6696	4.765	1.244
1536	4779.106	3.28	6734	4.752	1.257
1544	4805.307	3.27	6772	4.739	1.271
1552	4831.429	3.26	6810	4.726	1.284
1560	4857.469	3.25	6848	4.712	1.298
1568	4883.428	3.24	6886	4.699	1.311
1576	4909.303	3.229	6923	4.685	1.324
1584	4935.094	3.219	6961	4.671	1.337
1592	4960.799	3.208	6998	4.657	1.35
1600	4986.419	3.197	7035	4.643	1.363
1608	5011.951	3.186	7072	4.628	1.376
1616	5037.396	3.175	7109	4.613	1.389
1624	5062.753	3.164	7146	4.599	1.402
1632	5088.02	3.153	7183	4.584	1.415
1640	5113.197	3.141	7219	4.569	1.427
1648	5138.283	3.13	7256	4.553	1.44
1656	5163.279	3.119	7292	4.538	1.452
1664	5188.182	3.107	7328	4.523	1.465
1672	5212.994	3.096	7364	4.507	1.477
1680	5237.713	3.084	7400	4.491	1.489
1688	5262.339	3.072	7436	4.476	1.502
1696	5286.871	3.061	7472	4.46	1.514
1704	5311.31	3.049	7508	4.444	1.526

SAO Annual Report #3, NASA Grant NAG8-1605

1712	5335.655	3.037	7543	4.428	1.538
1720	5359.906	3.026	7579	4.412	1.55
1728	5384.063	3.014	7614	4.396	1.562
1736	5408.126	3.002	7649	4.38	1.574
1744	5432.095	2.99	7684	4.364	1.586
1752	5455.969	2.978	7719	4.348	1.597
1760	5479.75	2.967	7753	4.332	1.609
1768	5503.436	2.955	7788	4.316	1.621
1776	5527.029	2.943	7822	4.301	1.632
1784	5550.528	2.932	7857	4.285	1.644
1792	5573.935	2.92	7891	4.269	1.656
1800	5597.248	2.908	7925	4.253	1.667
1808	5620.461	2.895	7959	4.234	1.678
1816	5643.564	2.881	7993	4.215	1.69
1824	5666.556	2.867	8027	4.196	1.701
1832	5689.439	2.854	8060	4.177	1.713
1840	5712.214	2.84	8093	4.158	1.724
1848	5734.88	2.826	8127	4.14	1.735
1856	5757.439	2.813	8160	4.121	1.746
1864	5779.891	2.8	8192	4.103	1.758
1872	5802.237	2.787	8225	4.084	1.769
1880	5824.479	2.774	8258	4.066	1.78
1888	5846.616	2.761	8290	4.048	1.791
1896	5868.651	2.748	8323	4.031	1.802
1904	5890.583	2.735	8355	4.013	1.813
1912	5912.415	2.723	8387	3.996	1.824
1920	5934.148	2.71	8419	3.979	1.835
1928	5955.782	2.698	8450	3.962	1.846
1936	5977.32	2.686	8482	3.945	1.857
1944	5998.762	2.674	8514	3.928	1.868
1952	6020.11	2.663	8545	3.912	1.879
1960	6041.365	2.651	8576	3.896	1.89
1968	6062.53	2.64	8607	3.881	1.901
1976	6083.605	2.629	8638	3.865	1.912
1984	6104.593	2.618	8669	3.85	1.923
1992	6125.495	2.608	8700	3.836	1.934
2000	6146.313	2.597	8731	3.821	1.945
2008	6167.049	2.587	8761	3.807	1.956
2016	6187.704	2.577	8791	3.794	1.967
2024	6208.282	2.567	8822	3.78	1.978
2032	6228.783	2.558	8852	3.767	1.988
2040	6249.21	2.549	8882	3.755	1.999
2048	6269.566	2.54	8912	3.743	2.01
2056	6289.852	2.532	8942	3.731	2.021
2064	6310.07	2.523	8972	3.719	2.032
2072	6330.223	2.515	9001	3.709	2.043
2080	6350.315	2.508	9031	3.698	2.054
2088	6370.345	2.5	9061	3.688	2.065
2096	6390.319	2.493	9090	3.678	2.076
2104	6410.236	2.486	9119	3.669	2.087
2112	6430.102	2.48	9149	3.661	2.098
2120	6449.918	2.474	9178	3.653	2.109
2128	6469.687	2.468	9207	3.645	2.12
2136	6489.411	2.463	9236	3.638	2.131
2144	6509.094	2.458	9265	3.631	2.142
2152	6528.738	2.453	9294	3.625	2.153
2160	6548.347	2.449	9323	3.62	2.164
2168	6567.923	2.445	9352	3.615	2.175

SAO Annual Report #3, NASA Grant NAG8-1605

2176	6587.469	2.441	9381	3.61	2.186
2184	6606.988	2.438	9410	3.606	2.197
2192	6626.484	2.436	9439	3.603	2.209
2200	6645.96	2.433	9468	3.601	2.22
2208	6665.419	2.431	9497	3.598	2.231
2216	6684.863	2.43	9525	3.597	2.242
2224	6704.296	2.429	9554	3.596	2.254
2232	6723.723	2.428	9583	3.596	2.265
2240	6743.145	2.428	9612	3.596	2.276
2248	6762.567	2.428	9640	3.597	2.288
2256	6781.991	2.428	9669	3.599	2.299
2264	6801.421	2.429	9698	3.601	2.311
2272	6820.861	2.431	9727	3.604	2.322
2280	6840.315	2.433	9756	3.607	2.334
2288	6859.785	2.435	9785	3.612	2.345
2296	6879.275	2.438	9813	3.616	2.357
2304	6898.789	2.441	9842	3.622	2.369
2312	6918.331	2.445	9871	3.628	2.381
2320	6937.903	2.449	9900	3.635	2.394
2328	6957.51	2.453	9930	3.642	2.408
2336	6977.153	2.458	9959	3.65	2.423
2344	6996.836	2.463	9988	3.659	2.439
2352	7016.562	2.468	10017	3.668	2.455
2360	7036.332	2.474	10047	3.677	2.472
2368	7056.149	2.48	10076	3.687	2.489
2376	7076.014	2.486	10106	3.697	2.508
2384	7095.93	2.493	10135	3.707	2.527
2392	7115.898	2.499	10165	3.718	2.546
2400	7135.919	2.506	10195	3.728	2.566
2408	7155.993	2.513	10225	3.739	2.587
2416	7176.123	2.52	10255	3.75	2.608
2424	7196.308	2.527	10285	3.762	2.63
2432	7216.549	2.534	10315	3.773	2.652
2440	7236.845	2.54	10345	3.784	2.675
2448	7257.197	2.547	10375	3.795	2.698
2456	7277.604	2.554	10406	3.806	2.722
2464	7298.066	2.561	10436	3.817	2.746
2472	7318.581	2.568	10467	3.828	2.771
2480	7339.148	2.574	10497	3.838	2.796
2488	7359.765	2.58	10528	3.849	2.821
2496	7380.432	2.586	10559	3.858	2.847
2504	7401.145	2.592	10590	3.868	2.873
2512	7421.902	2.597	10621	3.877	2.9
2520	7442.701	2.602	10652	3.885	2.926
2528	7463.539	2.607	10683	3.893	2.954
2536	7484.412	2.611	10714	3.9	2.981
2544	7505.318	2.615	10745	3.907	3.009
2552	7526.251	2.618	10777	3.912	3.037
2560	7547.209	2.621	10808	3.917	3.065
2568	7568.186	2.623	10839	3.922	3.093
2576	7589.179	2.625	10871	3.925	3.122
2584	7610.183	2.626	10902	3.927	3.151
2592	7631.19	2.626	10934	3.929	3.18
2600	7652.198	2.626	10965	3.929	3.209
2608	7673.201	2.625	10997	3.928	3.238
2616	7694.192	2.623	11028	3.927	3.268
2624	7715.165	2.62	11059	3.924	3.297
2632	7736.115	2.617	11091	3.919	3.327

SAO Annual Report #3, NASA Grant NAG8-1605

2640	7757.034	2.613	11122	3.914	3.356
2648	7777.915	2.608	11153	3.908	3.386
2656	7798.754	2.602	11185	3.9	3.416
2664	7819.542	2.595	11216	3.89	3.446
2672	7840.272	2.587	11247	3.88	3.476
2680	7860.937	2.579	11278	3.868	3.506
2688	7881.529	2.569	11309	3.854	3.535
2696	7902.042	2.559	11339	3.84	3.565
2704	7922.469	2.547	11370	3.823	3.595
2712	7942.801	2.535	11401	3.806	3.625
2720	7963.031	2.522	11431	3.787	3.655
2728	7983.151	2.508	11461	3.767	3.684
2736	8003.156	2.493	11491	3.745	3.714
2744	8023.037	2.477	11521	3.722	3.743
2752	8042.788	2.46	11551	3.697	3.772
2760	8062.4	2.443	11580	3.672	3.801
2768	8081.867	2.424	11610	3.645	3.83
2776	8101.184	2.405	11639	3.616	3.859
2784	8120.343	2.385	11667	3.587	3.888
2792	8139.336	2.364	11696	3.556	3.916
2800	8158.162	2.342	11724	3.524	3.944
2808	8176.811	2.32	11752	3.492	3.972
2816	8195.279	2.297	11780	3.458	4
2824	8213.563	2.273	11808	3.423	4.027
2832	8231.654	2.249	11835	3.388	4.055
2840	8249.551	2.225	11862	3.351	4.082
2848	8267.249	2.2	11889	3.314	4.108
2856	8284.746	2.174	11915	3.276	4.135
2864	8302.038	2.149	11941	3.238	4.161
2872	8319.123	2.122	11967	3.2	4.186
2880	8335.998	2.096	11992	3.161	4.212
2888	8352.663	2.07	12017	3.121	4.237
2896	8369.117	2.043	12042	3.082	4.261
2904	8385.357	2.017	12067	3.043	4.285
2912	8401.388	1.991	12091	3.003	4.309
2920	8417.208	1.964	12115	2.964	4.333
2928	8432.819	1.938	12138	2.925	4.356
2936	8448.222	1.913	12161	2.887	4.378
2944	8463.421	1.887	12184	2.849	4.4
2952	8478.419	1.862	12207	2.812	4.422
2960	8493.222	1.838	12229	2.776	4.443
2968	8507.831	1.814	12252	2.741	4.464
2976	8522.254	1.791	12273	2.707	4.484
2984	8536.497	1.769	12295	2.673	4.504
2992	8550.564	1.748	12316	2.642	4.524
3000	8564.468	1.728	12337	2.611	4.543
3008	8578.209	1.708	12358	2.582	4.562
3016	8591.799	1.69	12378	2.555	4.58
3024	8605.245	1.672	12399	2.528	4.598
3032	8618.556	1.656	12419	2.504	4.616
3040	8631.74	1.641	12439	2.482	4.634
3048	8644.81	1.627	12459	2.461	4.651
3056	8657.771	1.614	12478	2.442	4.668
3064	8670.634	1.602	12498	2.425	4.684
3072	8683.411	1.592	12517	2.41	4.7
3080	8696.113	1.584	12536	2.397	4.716
3088	8708.752	1.576	12555	2.386	4.731
3096	8721.335	1.57	12574	2.377	4.747

SAO Annual Report #3, NASA Grant NAG8-1605

3104	8733.877	1.566	12593	2.371	4.761
3112	8746.389	1.563	12612	2.367	4.776
3120	8758.882	1.561	12631	2.365	4.79
3128	8771.37	1.561	12650	2.365	4.804
3136	8783.866	1.563	12669	2.368	4.817
3144	8796.378	1.566	12688	2.373	4.83
3152	8808.923	1.571	12707	2.38	4.843
3160	8821.513	1.577	12726	2.39	4.856
3168	8834.161	1.585	12745	2.403	4.868
3176	8846.877	1.594	12765	2.418	4.88
3184	8859.677	1.606	12784	2.435	4.891
3192	8872.571	1.618	12804	2.454	4.902
3200	8885.575	1.633	12823	2.477	4.913
3208	8898.699	1.648	12843	2.501	4.924
3216	8911.956	1.666	12863	2.528	4.934
3224	8925.356	1.685	12884	2.557	4.944
3232	8938.915	1.705	12904	2.588	4.953
3240	8952.644	1.727	12925	2.621	4.963
3248	8966.551	1.75	12946	2.657	4.972
3256	8980.648	1.775	12968	2.695	4.98
3264	8994.947	1.801	12989	2.734	4.989
3272	9009.458	1.827	13011	2.776	4.997
3280	9024.19	1.856	13034	2.819	5.004
3288	9039.155	1.885	13056	2.864	5.012
3296	9054.356	1.916	13080	2.911	5.019
3304	9069.806	1.947	13103	2.959	5.025
3312	9085.512	1.98	13127	3.009	5.032
3320	9101.479	2.013	13151	3.06	5.038
3328	9117.718	2.047	13176	3.112	5.044
3336	9134.229	2.082	13201	3.166	5.049
3344	9151.023	2.117	13227	3.22	5.054
3352	9168.099	2.152	13252	3.274	5.059
3360	9185.448	2.186	13279	3.327	5.064
3368	9203.074	2.22	13306	3.379	5.068
3376	9220.969	2.254	13333	3.431	5.072
3384	9239.13	2.287	13361	3.482	5.076
3392	9257.555	2.319	13389	3.532	5.079
3400	9276.239	2.352	13417	3.582	5.082
3408	9295.179	2.383	13446	3.631	5.085
3416	9314.371	2.415	13475	3.68	5.087
3424	9333.813	2.446	13505	3.728	5.089
3432	9353.503	2.476	13535	3.775	5.091
3440	9373.434	2.507	13565	3.822	5.093
3448	9393.606	2.536	13596	3.869	5.094
3456	9414.015	2.566	13627	3.914	5.095
3464	9434.658	2.595	13659	3.96	5.095
3472	9455.533	2.624	13691	4.004	5.096
3480	9476.636	2.652	13723	4.049	5.096
3488	9497.966	2.68	13755	4.093	5.095
3496	9519.52	2.708	13788	4.136	5.095
3504	9541.295	2.736	13821	4.179	5.094
3512	9563.29	2.763	13855	4.222	5.093
3520	9585.502	2.79	13889	4.264	5.091
3528	9607.93	2.817	13923	4.306	5.089
3536	9630.569	2.843	13958	4.348	5.087
3544	9653.422	2.87	13993	4.389	5.085
3552	9676.482	2.896	14028	4.43	5.082
3560	9699.751	2.921	14064	4.471	5.079

SAO Annual Report #3, NASA Grant NAG8-1605

3568	9723.226	2.947	14100	4.511	5.076
3576	9746.906	2.973	14136	4.551	5.072
3584	9770.789	2.998	14172	4.591	5.068
3592	9794.874	3.023	14209	4.631	5.064
3600	9819.158	3.048	14247	4.671	5.06
3608	9843.643	3.073	14284	4.71	5.055
3616	9868.33	3.098	14322	4.749	5.05
3624	9893.209	3.122	14360	4.788	0.5
3632	9918.271	3.144	14399	4.822	0.5
3640	9943.764	3.349	14438	5.138	0.5
3648	9972.842	3.915	14482	6.009	0.5
3656	10006.35	4.479	14534	6.877	0.5
3664	10044.45	5.04	14592	7.741	0.5
3672	10087.06	5.598	14658	8.603	0.5
3680	10134	6.139	14736	7.97	0.5
3688	10184.6	6.523	14802	8.593	0.5
3696	10238.25	6.878	14873	9.2	0.5
3704	10294.66	7.222	14949	9.813	0.5
3712	10353.75	7.546	15030	10.421	0.5
3720	10415.34	7.85	15116	11.024	0.5
3728	10479.28	8.135	15206	11.62	0.5
3736	10545.44	8.4	15302	12.209	0.5
3744	10613.65	8.645	15402	12.788	0.5
3752	10683.73	8.871	15506	13.356	0.5
3760	10755.53	9.078	15615	13.913	0.5
3768	10828.9	9.265	15729	14.456	0.5
3776	10903.72	9.434	15847	14.986	0.5
3784	10979.81	9.585	15969	15.501	0.5
3792	11057.04	9.718	16095	16	0.5
3800	11135.25	9.835	16224	16.483	0.5
3808	11214.34	9.936	16358	16.948	0.5
3816	11294.18	10.021	16496	17.395	0.5
3824	11374.64	10.091	16636	17.823	0.5
3832	11455.61	10.148	16781	18.234	0.5
3840	11536.97	10.191	16928	18.624	0.5
3848	11618.62	10.222	17079	18.995	0.5
3856	11700.49	10.241	17232	19.347	0.5
3864	11782.46	10.249	17388	19.679	0.5
3872	11864.44	10.247	17547	19.992	0.5
3880	11946.38	10.235	17708	20.285	0.5
3888	12028.18	10.215	17871	20.561	0.5
3896	12109.79	10.185	18037	20.814	0.5
3904	12191.14	10.149	18204	21.052	0.5
3912	12272.15	10.105	18374	21.269	0.5
3920	12352.79	10.054	18545	21.468	0.5
3928	12432.99	9.997	18717	21.649	0.5
3936	12512.73	9.935	18891	21.813	0.5
3944	12591.94	9.867	19066	21.959	0.5
3952	12670.59	9.795	19242	22.089	0.5
3960	12748.65	9.718	19419	22.202	0.5
3968	12826.07	9.637	19597	22.299	0.5
3976	12902.83	9.553	19776	22.381	0.5
3984	12978.91	9.465	19955	22.447	0.5
3992	13054.27	9.374	20135	22.497	0.5
4000	13128.89	9.28	20315	22.533	0.5
4008	13202.75	9.184	20496	22.555	0.5
4016	13275.83	9.085	20676	22.563	0.5
4024	13348.11	8.984	20857	22.557	0.5

SAO Annual Report #3, NASA Grant NAG8-1605

4032	13419.57	8.881	21037	22.537	0.5
4040	13490.19	8.776	21217	22.504	0.5
4048	13559.97	8.669	21397	22.458	0.5
4056	13628.89	8.56	21577	22.399	0.5
4064	13696.93	8.45	21756	22.327	0.5
4072	13764.08	8.338	21934	22.243	0.5
4080	13830.33	8.224	22111	22.145	0.5
4088	13895.66	8.109	22288	22.036	0.5
4096	13960.07	7.993	22464	21.913	0.5
4104	14023.54	7.875	22639	21.778	0.5
4112	14086.06	7.755	22812	21.63	0.5
4120	14147.62	7.634	22985	21.47	0.5
4128	14208.2	7.511	23156	21.297	0.5
4136	14267.8	7.387	23325	21.11	0.5
4144	14326.39	7.261	23494	20.91	0.5
4152	14383.96	7.133	23660	20.696	0.5
4160	14440.5	7.002	23825	20.467	0.5
4168	14495.99	6.87	23987	20.224	0.5
4176	14550.41	6.735	24148	19.965	0.5
4184	14603.75	6.598	24307	19.691	0.5
4192	14655.97	6.457	24463	19.399	0.5
4200	14707.05	6.314	24617	19.09	0.5
4208	14756.98	6.167	24769	18.761	0.5
4216	14805.71	6.016	24917	18.413	0.5
4224	14853.22	5.86	25063	18.042	0.5
4232	14899.47	5.7	25206	17.648	0.5
4240	14944.41	5.534	25345	17.227	0.5
4248	14987.99	5.361	25481	16.778	0.5
4256	15030.18	5.18	25912	23.014	0.66875
4264	15070.87	4.992	26101	24.046	0.96875
4272	15110.02	4.805	26296	24.87	1.25
4280	15147.86	4.656	26499	25.719	1.25
4288	15184.61	4.535	26708	26.581	1.25
4296	15212	4.437	26878	27.472	1.25
4304	15212	0	26878	0	1.25
4312	15212	0	26878	0	1.25
4320	15212	0	26878	0	1.25
4328	15212	0	26878	0	1.25
4336	15212	0	26878	0	1.25
4344	15212	0	26878	0	1.25
4352	15212	0	26878	0	1.25
4360	15212	0	26878	0	1.25
4368	15212	0	26878	0	1.25
4376	15212	0	26878	0	1.25
4384	15212	0	26878	0	1.25
4392	15212	0	26878	0	1.25
4400	15212	0	26878	0	1.25
4408	15212	0	26878	0	1.25
4416	15212	0	26878	0	1.25
4424	15212	0	26878	0	1.23843
4432	15212	0	26878	0	1.20138
4440	15212	0	26878	0	1.16434
4448	15212	0	26878	0	1.12731
4456	15212	0	26878	0	1.09027
4464	15212	0	26878	0	1.05323
4472	15212	0	26878	0	1.01619
4480	15212	0	26878	0	0.979145
4488	15212	0	26878	0	0.942105

SAO Annual Report #3, NASA Grant NAG8-1605

4496	15212	0	26878	0	0.905065
4504	15212	0	26878	0	0.868025
4512	15212	0	26878	0	0.830985
4520	15212	0	26878	0	0.793945
4528	15212	0	26878	0	0.756905
4536	15212	0	26878	0	0.719865
4544	15212	0	26878	0	0.682825
4552	15212	0	26878	0	0.645785
4560	15212	0	26878	0	0.608745
4568	15212	0	26878	0	0.571705
4576	15212	0	26878	0	0.534665
4584	15212	0	26878	0	0.497625
4592	15212	0	26878	0	0.460585
4600	15212	0	26878	0	0.423545
4608	15212	0	26878	0	0.386505
4616	15212	0	26878	0	0.349465
4624	15212	0	26878	0	0.312425
4632	15212	0	26878	0	0.275385
4640	15212	0	26878	0	0.238345
4648	15212	0	26878	0	0.201305
4656	15212	0	26878	0	0.164265
4664	15212	0	26878	0	0.127225
4672	15212	0	26878	0	0.090185
4680	15212	0	26878	0	0.053145
4688	15212	0	26878	0	0.016105
4696	15212	0	26878	0	0
4704	15212	0	26878	0	0
4712	15212	0	26878	0	0
4720	15212	0	26878	0	0
4728	15212	0	26878	0	0
4736	15212	0	26878	0	0
4744	15212	0	26878	0	0
4752	15212	0	26878	0	0
4760	15212	0	26878	0	0
4768	15212	0	26878	0	0
4776	15212	0	26878	0	0
4784	15212	0	26878	0	0
4792	15212	0	26878	0	0
4800	15212	0	26878	0	0
4808	15212	0	26878	0	0
4816	15212	0	26878	0	0
4824	15212	0	26878	0	0
4832	15212	0	26878	0	0
4840	15212	0	26878	0	0
4848	15212	0	26878	0	0
4856	15212	0	26878	0	0
4864	15212	0	26878	0	0
4872	15212	0	26878	0	0
4880	15212	0	26878	0	0
4888	15212	0	26878	0	0
4896	15212	0	26878	0	0
4904	15212	0	26878	0	0
4912	15212	0	26878	0	0
4920	15212	0	26878	0	0
4928	15212	0	26878	0	0
4936	15212	0	26878	0	0
4944	15212	0	26878	0	0
4952	15212	0	26878	0	0

SAO Annual Report #3, NASA Grant NAG8-1605

4960	15212	0	26878	0	0
4968	15212	0	26878	0	0
4976	15212	0	26878	0	0
4984	15212	0	26878	0	0
4992	15212	0	26878	0	0
5000	15212	0	26878	0	0
5008	15212	0	26878	0	0
5016	15212	0	26878	0	0
5024	15212	0	26878	0	0
5032	15212	0	26878	0	0
5040	15212	0	26878	0	0
5048	15212	0	26878	0	0
5056	15212	0	26878	0	0
5064	15212	0	26878	0	0
5072	15212	0	26878	0	0
5080	15212	0	26878	0	0
5088	15212	0	26878	0	0
5096	15212	0	26878	0	0
5104	15212	0	26878	0	0
5112	15212	0	26878	0	0
5120	15212	0	26878	0	0
5128	15212	0	26878	0	0
5136	15212	0	26878	0	0
5144	15212	0	26878	0	0
5152	15212	0	26878	0	0
5160	15212	0	26878	0	0
5168	15212	0	26878	0	0
5176	15212	0	26878	0	0
5184	15212	0	26878	0	0
5192	15212	0	26878	0	0
5200	15212	0	26878	0	0
5208	15212	0	26878	0	0
5216	15212	0	26878	0	0
5224	15212	0	26878	0	0
5232	15212	0	26878	0	0
5240	15212	0	26878	0	0
5248	15212	0	26878	0	0
5256	15212	0	26878	0	0
5264	15212	0	26878	0	0
5272	15212	0	26878	0	0
5280	15212	0	26878	0	0
5288	15212	0	26878	0	0
5296	15212	0	26878	0	0
5304	15212	0	26878	0	0
5312	15212	0	26878	0	0
5320	15212	0	26878	0	0
5328	15212	0	26878	0	0
5336	15212	0	26878	0	0
5344	15212	0	26878	0	0
5352	15212	0	26878	0	0
5360	15212	0	26878	0	0
5368	15212	0	26878	0	0
5376	15212	0	26878	0	0
5384	15212	0	26878	0	0
5392	15212	0	26878	0	0
5400	15212	0	26878	0	0
5408	15212	0	26878	0	0
5416	15212	0	26878	0	0

SAO Annual Report #3, NASA Grant NAG8-1605

5424	15212	0	26878	0	0
5432	15212	0	26878	0	0
5440	15212	0	26878	0	0
5448	15212	0	26878	0	0
5456	15212	0	26878	0	0
5464	15212	0	26878	0	0
5472	15212	0	26878	0	0
5480	15212	0	26878	0	0
5488	15212	0	26878	0	0
5496	15212	0	26878	0	0
5504	15212	0	26878	0	0
5512	15212	0	26878	0	0
5520	15212	0	26878	0	0
5528	15212	0	26878	0	0
5536	15212	0	26878	0	0
5544	15212	0	26878	0	0
5552	15212	0	26878	0	0
5560	15212	0	26878	0	0
5568	15212	0	26878	0	0
5576	15212	0	26878	0	0
5584	15212	0	26878	0	0
5592	15212	0	26878	0	0
5600	15212	0	26878	0	0
5608	15212	0	26878	0	0
5616	15212	0	26878	0	0
5624	15212	0	26878	0	0
5632	15212	0	26878	0	0
5640	15212	0	26878	0	0
5648	15212	0	26878	0	0
5656	15212	0	26878	0	0
5664	15212	0	26878	0	0
5672	15212	0	26878	0	0
5680	15212	0	26878	0	0
5688	15212	0	26878	0	0
5696	15212	0	26878	0	0
5704	15212	0	26878	0	0
5712	15212	0	26878	0	0
5720	15212	0	26878	0	0
5728	15212	0	26878	0	0
5736	15212	0	26878	0	0
5744	15212	0	26878	0	0
5752	15212	0	26878	0	0
5760	15212	0	26878	0	0
5768	15212	0	26878	0	0
5776	15212	0	26878	0	0
5784	15212	0	26878	0	0
5792	15212	0	26878	0	0
5800	15212	0	26878	0	0
5808	15212	0	26878	0	0
5816	15212	0	26878	0	0
5824	15212	0	26878	0	0
5832	15212	0	26878	0	0
5840	15212	0	26878	0	0
5848	15212	0	26878	0	0
5856	15212	0	26878	0	0
5864	15212	0	26878	0	0
5872	15212	0	26878	0	0
5880	15212	0	26878	0	0

SAO Annual Report #3, NASA Grant NAG8-1605

5888	15212	0	26878	0	0
5896	15212	0	26878	0	0
5904	15212	0	26878	0	0
5912	15212	0	26878	0	0
5920	15212	0	26878	0	0
5928	15212	0	26878	0	0
5936	15212	0	26878	0	0
5944	15212	0	26878	0	0
5952	15212	0	26878	0	0
5960	15212	0	26878	0	0
5968	15212	0	26878	0	0
5976	15212	0	26878	0	0
5984	15212	0	26878	0	0
5992	15212	0	26878	0	0
6000	15212	0	26878	0	0
6008	15212	0	26878	0	0
6016	15212	0	26878	0	0
6024	15212	0	26878	0	0
6032	15212	0	26878	0	0
6040	15212	0	26878	0	0
6048	15212	0	26878	0	0
6056	15212	0	26878	0	0
6064	15212	0	26878	0	0
6072	15212	0	26878	0	0
6080	15212	0	26878	0	0
6088	15212	0	26878	0	0
6096	15212	0	26878	0	0
6104	15212	0	26878	0	0
6112	15212	0	26878	0	0
6120	15212	0	26878	0	0
6128	15212	0	26878	0	0
6136	15212	0	26878	0	0
6144	15212	0	26878	0	0
6152	15212	0	26878	0	0
6160	15212	0	26878	0	0
6168	15212	0	26878	0	0
6176	15212	0	26878	0	0
6184	15212	0	26878	0	0
6192	15212	0	26878	0	0
6200	15212	0	26878	0	0
6208	15212	0	26878	0	0
6216	15212	0	26878	0	0
6224	15212	0	26878	0	0
6232	15212	0	26878	0	0
6240	15212	0	26878	0	0
6248	15212	0	26878	0	0
6256	15212	0	26878	0	0
6264	15212	0	26878	0	0
6272	15212	0	26878	0	0
6280	15212	0	26878	0	0
6288	15212	0	26878	0	0
6296	15212	0	26878	0	0
6304	15212	0	26878	0	0
6312	15212	0	26878	0	0
6320	15212	0	26878	0	0
6328	15212	0	26878	0	0
6336	15212	0	26878	0	0
6344	15212	0	26878	0	0

SAO Annual Report #3, NASA Grant NAG8-1605

6352	15212	0	26878	0	0
6360	15212	0	26878	0	0
6368	15212	0	26878	0	0
6376	15212	0	26878	0	0
6384	15212	0	26878	0	0
6392	15212	0	26878	0	0
6400	15212	0	26878	0	0
6408	15212	0	26878	0	0
6416	15212	0	26878	0	0
6424	15212	0	26878	0	0
6432	15212	0	26878	0	0
6440	15212	0	26878	0	0
6448	15212	0	26878	0	0
6456	15212	0	26878	0	0
6464	15212	0	26878	0	0
6472	15212	0	26878	0	0
6480	15212	0	26878	0	0
6488	15212	0	26878	0	0
6496	15212	0	26878	0	0
6504	15212	0	26878	0	0
6512	15212	0	26878	0	0
6520	15212	0	26878	0	0
6528	15212	0	26878	0	0
6536	15212	0	26878	0	0
6544	15212	0	26878	0	0
6552	15212	0	26878	0	0
6560	15212	0	26878	0	0
6568	15212	0	26878	0	0
6576	15212	0	26878	0	0
6584	15212	0	26878	0	0
6592	15212	0	26878	0	0
6600	15212	0	26878	0	0
6608	15212	0	26878	0	0
6616	15212	0	26878	0	0
6624	15212	0	26878	0	0
6632	15212	0	26878	0	0
6640	15212	0	26878	0	0
6648	15212	0	26878	0	0
6656	15212	0	26878	0	0
6664	15212	0	26878	0	0
6672	15212	0	26878	0	0
6680	15212	0	26878	0	0
6688	15212	0	26878	0	0
6696	15212	0	26878	0	0
6704	15212	0	26878	0	0
6712	15212	0	26878	0	0
6720	15212	0	26878	0	0
6728	15212	0	26878	0	0
6736	15212	0	26878	0	0
6744	15212	0	26878	0	0
6752	15212	0	26878	0	0
6760	15212	0	26878	0	0
6768	15212	0	26878	0	0
6776	15212	0	26878	0	0
6784	15212	0	26878	0	0
6792	15212	0	26878	0	0
6800	15212	0	26878	0	0
6808	15212	0	26878	0	0

SAO Annual Report #3, NASA Grant NAG8-1605

6816	15212	0	26878	0	0
6824	15212	0	26878	0	0
6832	15212	0	26878	0	0
6840	15212	0	26878	0	0
6848	15212	0	26878	0	0
6856	15212	0	26878	0	0
6864	15212	0	26878	0	0
6872	15212	0	26878	0	0
6880	15212	0	26878	0	0
6888	15212	0	26878	0	0
6896	15212	0	26878	0	0
6904	15212	0	26878	0	0
6912	15212	0	26878	0	0
6920	15212	0	26878	0	0
6928	15212	0	26878	0	0
6936	15212	0	26878	0	0
6944	15212	0	26878	0	0
6952	15212	0	26878	0	0
6960	15212	0	26878	0	0
6968	15212	0	26878	0	0
6976	15212	0	26878	0	0
6984	15212	0	26878	0	0
6992	15212	0	26878	0	0
7000	15212	0	26878	0	0
7008	15212	0	26878	0	0
7016	15212	0	26878	0	0
7024	15212	0	26878	0	0
7032	15212	0	26878	0	0
7040	15212	0	26878	0	0
7048	15212	0	26878	0	0
7056	15212	0	26878	0	0
7064	15212	0	26878	0	0
7072	15212	0	26878	0	0
7080	15212	0	26878	0	0
7088	15212	0	26878	0	0
7096	15212	0	26878	0	0
7104	15212	0	26878	0	0
7112	15212	0	26878	0	0
7120	15212	0	26878	0	0
7128	15212	0	26878	0	0
7136	15212	0	26878	0	0
7144	15212	0	26878	0	0
7152	15212	0	26878	0	0
7160	15212	0	26878	0	0
7168	15212	0	26878	0	0
7176	15212	0	26878	0	0
7184	15212	0	26878	0	0
7192	15212	0	26878	0	0
7200	15212	0	26878	0	0
*****		EOF	*****		

REFERENCES

- ¹ J.R. Sanmartin, M. Manuel-Martinez, and E. Ahedo, "Bare Wire Anodes for Electrodynamic Tethers." *J. of Propulsion and Power*, Vol. 9, No. 3, 353-360, 1993.
- ² R.D. Estes, J.R. Sanmartin, and M. Martinez-Sanchez, "Performance of Bare-Tethers Systems Under Varying magnetic and Plasma Conditions." *J. of Spacecraft and Rockets*, Vol. 37, No. 2, 197-204, 2000.
- ³ Estes, R.D., E.C. Lorenzini, J.R. Sanmartin, M. Martinez-Sanchez and N.A. Savich, "New High-Current Tethers: A Viable Power Source for the Space Station?," Smithsonian Astrophysical Observatory, White Paper, December 1995.
- ⁴ L. Johnson, R.D. Estes, E. Lorenzini, M. Martinez-Sanchez and J. Sanmartin "Propulsive Small Expendable Deployer System Experiment." *J. of Spacecraft and Rockets*, Vol. 37, No. 2, 173-176, 2000.
- ⁵ E.C. Lorenzini et al., "The Propulsive Small Expendable Deployer System (ProSEDS)." Annual Report#1 on NASA Grant NAG8-1605, September 2001.
- ⁶ J. Pelaez, E.C. Lorenzini, O. Lopez-Rebollal and M. Ruiz, "A New Kind of Dynamic Instability in Electrodynamic Tethers." The Journal of the Astronautical Sciences Vol. 48, No. 4, 449-476, 2000.
- ⁷ E.C. Lorenzini et al. "The Propulsive Small Expendable Deployer System (ProSEDS)." Annual Report #2 on NASA Grant NAG8-1605, July 2001.
- ⁸ Lorenzini, E.C., S. Bortolami, C.C. Rupp and F. Angrilli, "Control and Flight Performance of Tethered Satellite Small Expendable Deployment System-II" *Journal of Guidance, Control and Dynamics*, Vol. 19, No. 5, 1148-1156, 1996.